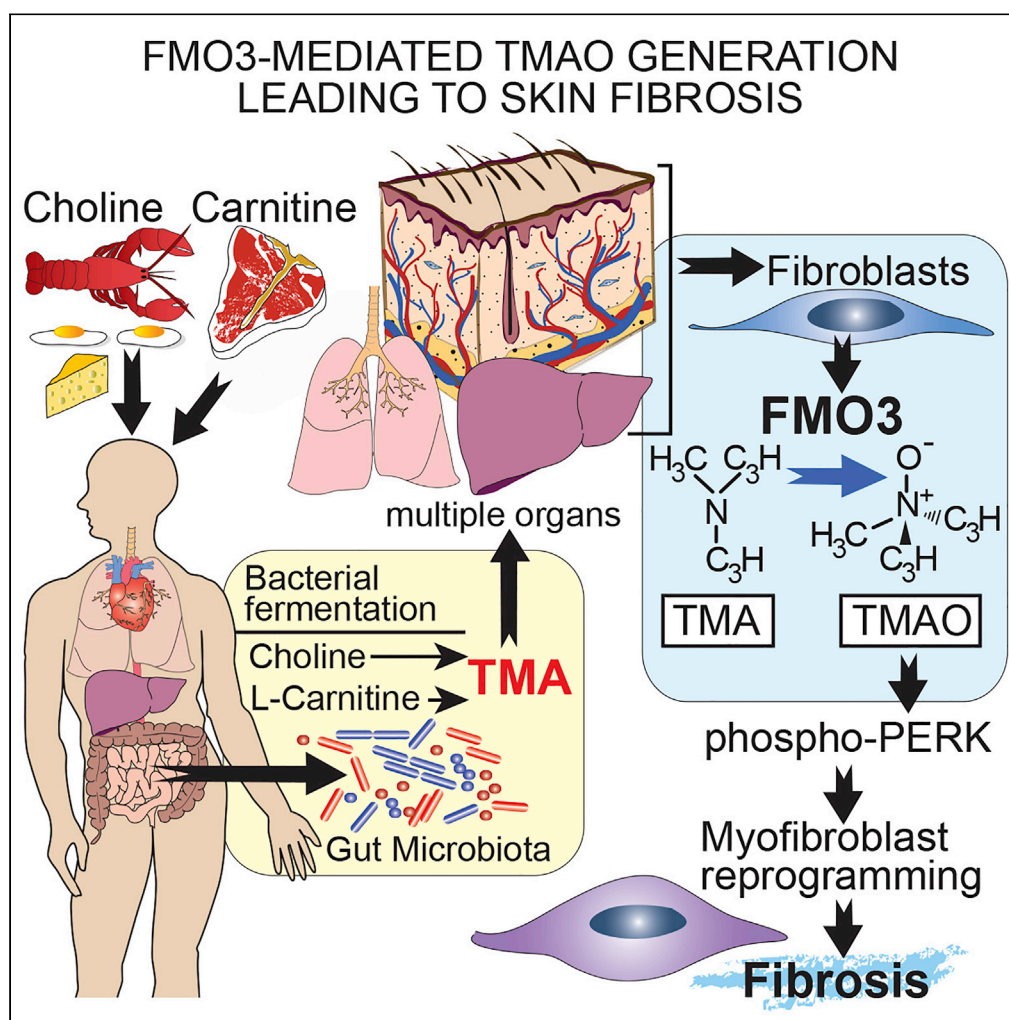


Article

Gut microbe-derived metabolite trimethylamine N-oxide activates PERK to drive fibrogenic mesenchymal differentiation



Seok-Jo Kim,
Swarna Bale,
Priyanka Verma,
..., Nilaksh Gupta,
Karen J. Ho, John
Varga

vargaj@med.umich.edu

Highlights

Reprogramming
mesenchymal progenitors
into myfibroblasts by
TMAO via PERK

FMO3 upregulation in SSc
skin fibroblasts

Article

Gut microbe-derived metabolite trimethylamine N-oxide activates PERK to drive fibrogenic mesenchymal differentiation

Seok-Jo Kim,^{1,2,11} Swarna Bale,^{1,11} Priyanka Verma,^{1,11} Qianqian Wan,¹ Feiyang Ma,^{3,9} Johann E. Gudjonsson,^{1,3} Stanley L. Hazen,^{4,5,6} Paul W. Harms,^{3,7} Pei-Suen Tsou,¹ Dinesh Khanna,^{1,8} Lam C. Tsoi,^{3,9} Nilaksh Gupta,^{4,5} Karen J. Ho,¹⁰ and John Varga^{1,3,8,12,*}

SUMMARY

Intestinal dysbiosis is prominent in systemic sclerosis (SSc), but it remains unknown how it contributes to microvascular injury and fibrosis that are hallmarks of this disease. Trimethylamine (TMA) is generated by the gut microbiome and in the host converted by flavin-containing monooxygenase (FMO3) into trimethylamine N-oxide (TMAO), which has been implicated in chronic cardiovascular and metabolic diseases. Using cell culture systems and patient biopsies, we now show that TMAO reprograms skin fibroblasts, vascular endothelial cells, and adipocytic progenitor cells into myofibroblasts via the putative TMAO receptor protein R-like endoplasmic reticulum kinase (PERK). Remarkably, FMO3 was detected in skin fibroblasts and its expression stimulated by TGF- β 1. Moreover, FMO3 was elevated in SSc skin biopsies and in SSc fibroblasts. A meta-organismal pathway thus might in SSc link gut microbiome to vascular remodeling and fibrosis via stromal cell reprogramming, implicating the FMO3-TMAO-PERK axis in pathogenesis, and as a promising target for therapy.

INTRODUCTION

Systemic sclerosis (SSc) is a poorly understood chronic orphan disease with variable progression, substantial mortality, and no effective therapy (Allanore et al., 2015; Denton and Khanna, 2017). The hallmarks of SSc are aberrant vascular and immune responses leading to intractable fibrosis (Bhattacharyya et al., 2012; Distler et al., 2019; Varga and Abraham, 2007). Although the etiology remains unknown, recent studies suggest a complex interplay of genetic factors and environmental exposures (Angiolilli et al., 2018). Widespread fibrosis synchronously affecting multiple organs, a distinguishing hallmark of SSc, is associated with persistent tissue accumulation of myofibroblasts (Hinz and Lagares, 2020). Multiple lines of evidence suggest that disease-associated myofibroblasts represent a reprogrammed fibrotic cell population originating from tissue-resident mesenchymal progenitors most prominently fibroblasts, vascular endothelial cells, pericytes and preadipocytes (Pakshir et al., 2020). Endothelial-to-mesenchymal transition (endoMT), in particular, has received considerable recent attention as the pathomechanistic process linking vasculopathy and fibrosis characteristic of SSc (Manetti et al., 2017; Piera-Velazquez et al., 2016).

The intestinal microbiome plays a fundamental role in shaping immunity, and its dysregulation (dysbiosis) is increasingly implicated in autoimmune diseases (Belkaid and Hand, 2014; Zhang et al., 2020). Recent studies have documented prominent intestinal dysbiosis in patients with SSc. However, the direct and indirect contributions of altered gut microbiome to vascular and matrix remodeling and other processes underlying clinical manifestations of SSc remain largely unknown (Patrone et al., 2017; Volkmann et al., 2017). Gut microbes metabolize dietary choline and carnitine, nutrients abundant in Western diet, to generate trimethylamine (TMA) (Koeth et al., 2013; Wang et al., 2011), which can be converted to trimethylamine N-oxide (TMAO) in the host (Organ et al., 2016; Tang et al., 2015; Wang et al., 2011). Notably, bacterial taxa enriched in SSc intestinal microbiota are known to be high TMA producers (Wu et al., 2019). The enzyme responsible for converting gut microbe-derived TMA to TMAO in the mammalian host is flavin-containing monooxygenase 3 (FMO3), which is expressed primarily in the liver (Bennett et al., 2013; Krueger and Williams, 2005). Elevated TMAO levels have been associated with metabolic syndrome, atherosclerosis, and other chronic

¹Division of Rheumatology, Department of Internal Medicine, The University of Michigan, Suite 7C27, 300 North Ingalls Building, Ann Arbor, MI, USA

²SCM Lifescience Co. Ltd., Incheon, Republic of Korea

³Department of Dermatology, The University of Michigan, 300 North Ingalls Building, Ann Arbor, MI, USA

⁴Department of Cardiovascular and Metabolic Sciences, Lerner Research Institute, Cleveland Clinic, Cleveland, OH, USA

⁵Center for Microbiome & Human Health, Cleveland Clinic, Cleveland, OH, USA

⁶Department of Cardiovascular Medicine, Heart and Vascular Institute, Cleveland Clinic, Cleveland, OH, USA

⁷Department of Pathology, The University of Michigan, Ann Arbor, MI, USA

⁸Michigan Scleroderma Program, The University of Michigan, 300 North Ingalls Building, Ann Arbor, MI, USA

⁹Department of Computational Medicine & Bioinformatics, The University of Michigan, Ann Arbor, MI, USA

¹⁰Department of Surgery, Northwestern University Feinberg School of Medicine, Chicago, IL, USA

¹¹These authors contributed equally

¹²Lead contact

*Correspondence: varga@med.umich.edu

<https://doi.org/10.1016/j.isci.2022.104669>



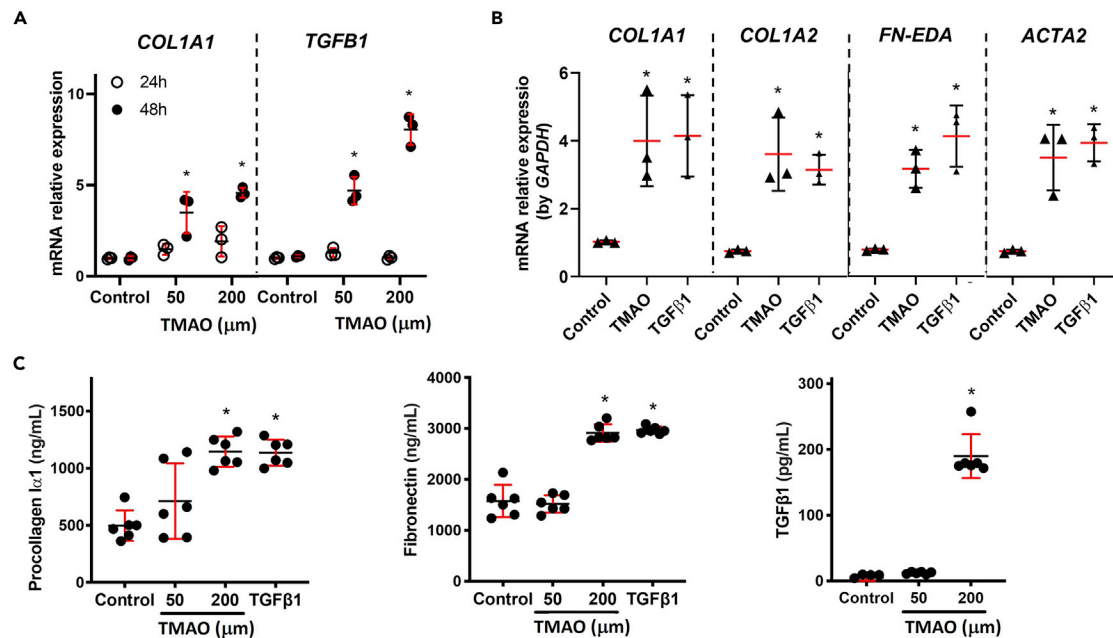


Figure 1. TMAO stimulates fibrotic gene expression in skin fibroblasts

Confluent cultures of normal skin fibroblasts were incubated with indicated concentrations of TMAO and/or TGF-β1 (5 ng/mL) for 48 h.

(A and B) Total RNA was subjected to real-time qPCR; results are means ± SEM of three independent determinations (*p < 0.05 versus control; n = 3).

(C) Media were assayed for procollagen Iα1, fibronectin and TGF-β1 by ELISA. Results are means ± SEM of three determinations. (*p < 0.05 versus control; n = 6).

vascular and degenerative diseases, and are increasingly recognized to play a direct pathogenic role in these chronic conditions (Janeiro et al., 2018; Witkowski et al., 2020).

The effects of TMAO on the hallmark vascular and fibrotic pathomechanisms underlying SSc are not well known. We demonstrate here that TMAO is a potent stimulus for differentiation of skin fibroblasts, endothelial cells and adipocytic progenitor cells into myofibroblasts. This process is mediated by the cellular enzyme R-like endoplasmic reticulum kinase (PERK), which binds directly to TMAO (Chen et al., 2019). We also show that the TMAO-generating enzyme FMO3 is detected and is active in skin fibroblasts and endothelial cells *in vitro* and *in vivo*, and its expression is induced by TGF-β1. Furthermore, FMO3 expression is elevated in isolated SSc skin fibroblasts and in SSc skin biopsies, where it maps primarily to fibroblasts and pericytes. These findings broaden the spectrum of recognized pathogenic activities associated with TMAO and uncover previously unsuspected effects for this gut microbe-derived metabolite in fibrosis, potentially implicating the FMO3-TMAO axis in SSc pathogenesis.

RESULTS

TMAO induced myofibroblast differentiation

To investigate the effect of TMAO on mesenchymal cell differentiation, a series of experiments were performed using isolated human cells incubated in media with or without TMAO. In confluent human fibroblasts, TMAO induced significant stimulation of *COL1A1*, *COL1A2*, *ACTA2*, and *FN-EDA* mRNA expression, accompanied by time- and dose-dependent increase in the secretion of procollagen I and fibronectin, as well as TGF-β1 (Figure 1). Furthermore, TMAO induced a substantial increase in cellular F-actin stress fibers and formation of focal adhesions, hallmarks of mature myofibroblasts, in quiescent fibroblasts (Figures 2 and S1). These profibrotic effects elicited by TMAO are unlikely to reflect autocrine fibroblast stimulation via endogenous TGF-β1, because in contrast to exogenous TGF-β1 treatment, TMAO failed to elicit activation of Smad2 in these cells (Figure S1). Interestingly, the gut microbiome-derived TMAO metabolic precursor TMA itself also induced activation of PERK and modest fibrotic responses, albeit only at relative high concentrations (Figure S2), suggesting that exogenous TMA might be converted to TMAO in a fibroblast-autonomous manner.

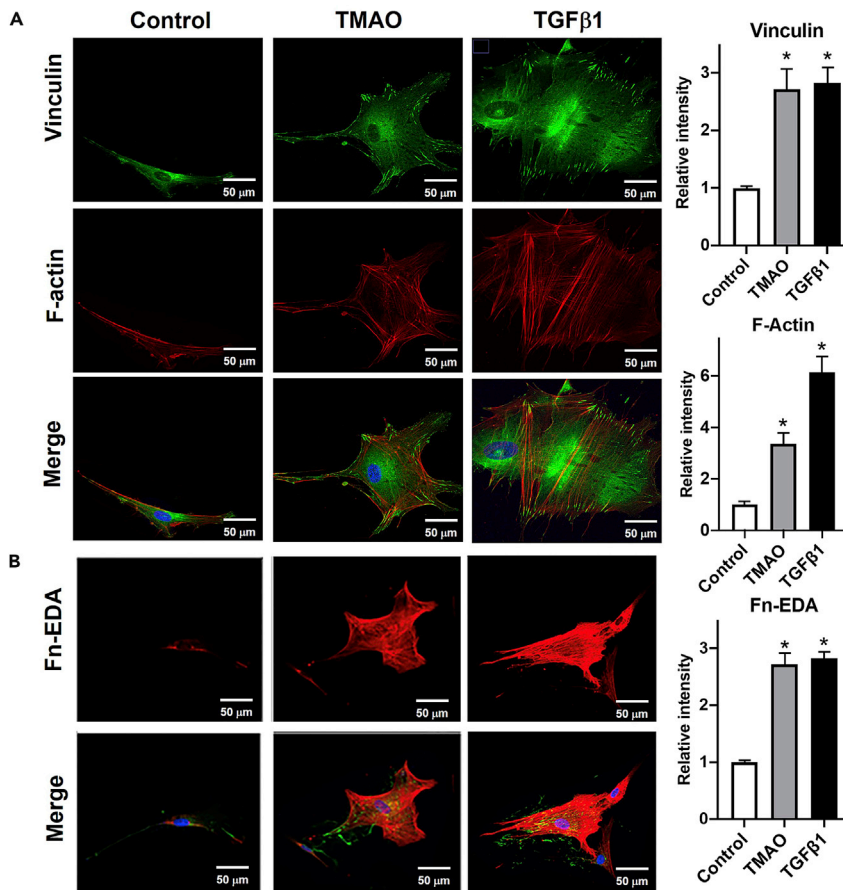


Figure 2. TMAO induces myofibroblast transition

(A and B) Confluent skin fibroblasts incubated with TMAO (200 μ M) or TGF- β 1 (5 ng/mL) for 48 h were immunolabeled with antibodies to (A) vinculin (green) and F-actin (red); (B) fibronectin-EDA (red). Nuclei were stained with DAPI (blue). Cells were viewed under an immunofluorescence microscope or a Nikon C2 or A1Si confocal microscope. Representative photomicrographs (right panels). Original magnification 400x. Images were analyzed by ImageJ. * $p < 0.05$ versus control; $n = 3$.

Upon injury, vascular endothelial cells characteristically undergo myofibroblast transdifferentiation through the process of endoMT (Bischoff, 2019). Profibrotic cellular reprogramming via endoMT is particularly salient to SSc as it represents a mechanism potentially linking the vascular and fibrotic pathologies characteristic of SSc (Di Benedetto et al., 2021; Jimenez, 2013). In light of the well-recognized vasculopathic effects of TMAO (Organ et al., 2020; Witkowski et al., 2020), we sought to investigate its effects on microvascular endothelial cell function. Incubation of HMVECs with TMAO markedly suppressed the expression of endothelial markers VE-cadherin (*CDH5*) and CD31 (*PECAM1*) while augmenting the expression of myofibroblast markers *COL1A1*, *ACTA2*, *SNAI2*, and *TAGLN* (Figures 3A and 3B). In parallel, TMAO significantly suppressed the levels of cellular CD31 protein while augmenting the levels of TAGLN and fibronectin extra-domain A (Figure 3C). Human umbilical vein endothelial cells (HUVECs) treated with TMAO *in vitro* displayed comparable changes, accompanied by loss of the characteristic cobblestone morphology (data not shown).

To identify molecular mechanisms underlying these striking profibrotic endothelial cell responses elicited by TMAO, RNA was isolated from HMVECs incubated in media with or without TMAO and subjected to RNA sequencing and genomewide transcriptome analysis followed by gene set enrichment analysis (GSEA). As shown in Figure 3, treatment of HMVECs with TMAO for 48 h induced substantial changes in gene expression, with upregulation of multiple mesenchymal-associated genes and concomitant suppression of endothelial genes (Figures 3D and 3E). To understand the potential impact of TMAO on fibrosis-related epigenetic alterations, we performed unbiased global histone H3 modification analysis. Confluent

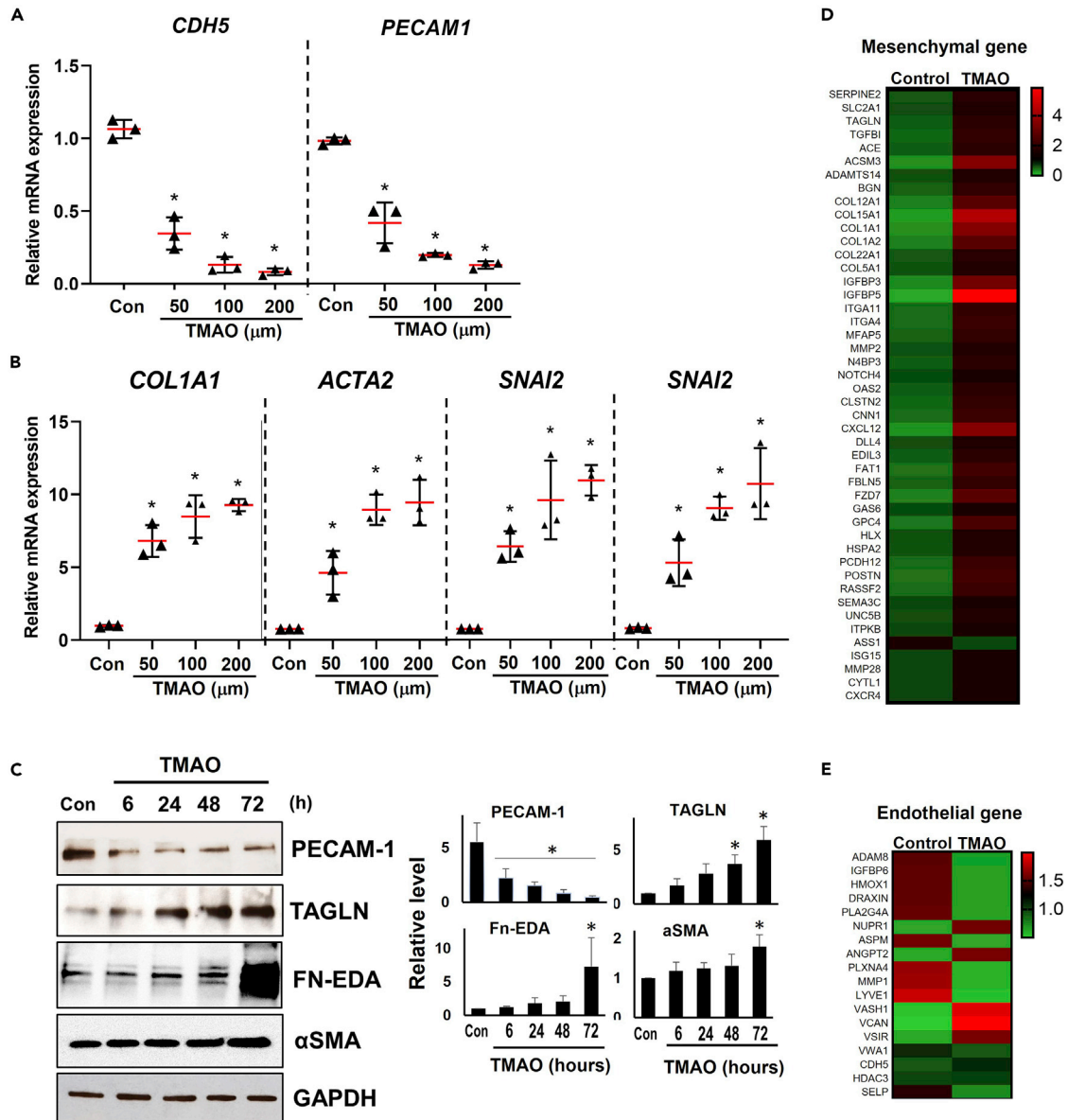


Figure 3. TMAO triggers endothelial-mesenchymal transition

Confluent HMVECs were incubated with TMAO at the indicated concentrations for 72 h.

(A and B) Total RNA was subjected to real-time qPCR. Results are means \pm SD of three determinations ($*p < 0.05$ versus control; $n = 3$).

(C) Whole cell lysates were subjected to immunoblotting; representative images (left). Results quantified using ImageJ (right) are representative of three independent experiments ($*p < 0.05$ versus control; $n = 3$).

(D and E) RNA-seq analysis. Heatmaps showing expression of mesenchymal (D) and endothelial (E)-related genes in untreated vs. TMAO-treated cells. ($p < 0.05$; $n = 3$).

HMVECs were incubated with TMAO (50 μM) for 48 h, followed by isolation of histone, binding to assay well and colorimetric detection of modified histones using EpiQuik multiplex assay kits according to the manufacturer's instructions.

The results showed significant upregulation in H3K4me3 and other H3 histone methylation marks in TMAO-treated compared with untreated control endothelial cells (Figure S3). These data suggest that TMAO triggers extensive chromatin remodeling in endothelial cells via modulating distinct histone marks that underlies its profibrotic effects.

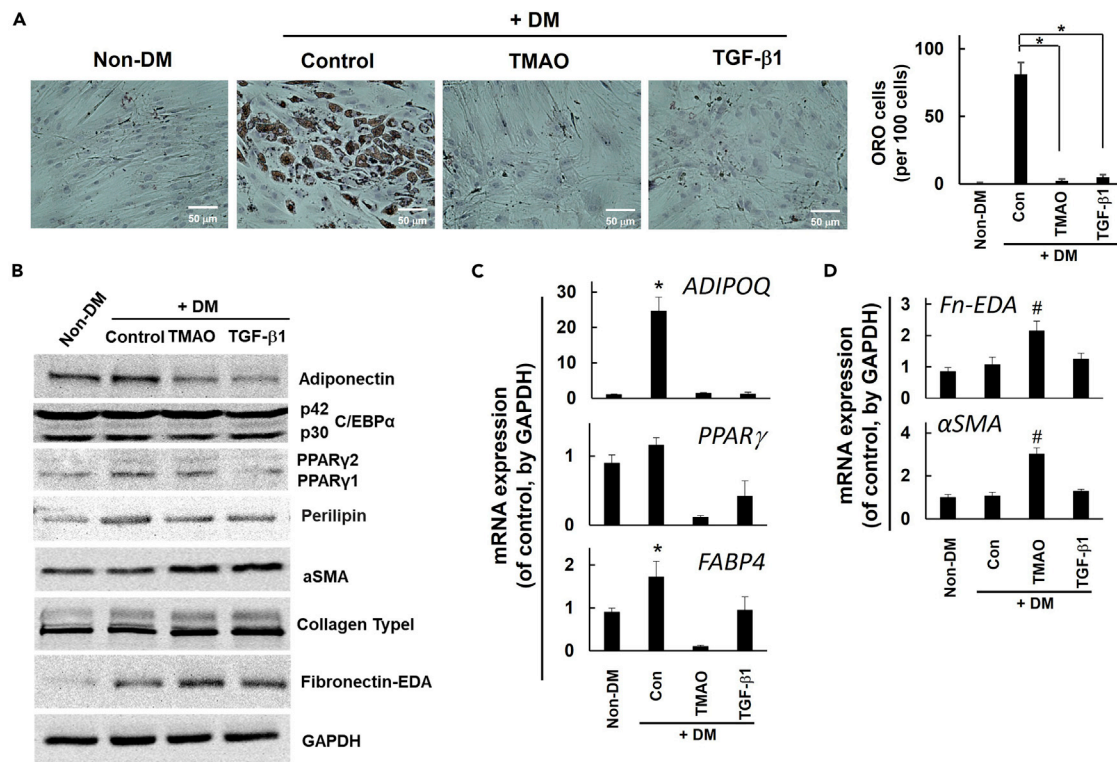


Figure 4. TMAO induces mesenchymal transition in adipocytes

Human subcutaneous adipose tissue-derived progenitor cells (ADSCs) were differentiated to adipocytes, and then incubated in differentiation media for 10 days in the presence of TMAO (100 μ M) or TGF- β 1 (10 ng/mL).

(A) Cells were stained with Oil Red O and counted (100 cells/well).

(B) Whole cell lysates were analyzed by immunoblotting. Representative images.

(C and D) Total RNA was subjected to RT-PCR. Results are representative of three independent experiments. (* $p < 0.05$ versus control; $n = 3$; # $p < 0.05$ versus control+DM; $n = 3$).

Because adipocytic progenitor cells can undergo fibrotic reprogramming into myofibroblasts through the process of adipocytic-mesenchymal transition (AMT), which had been implicated in dermal fibrosis in SSC (Marangoni et al., 2015; Varga and Marangoni, 2017), we examined the effect on TMAO on adipocyte differentiation. Cultures of human ADSCs were differentiated *in vitro* into mature adipocytes, identifiable by their characteristic rounded cell shape and prominent Oil-red-O-positive intracytoplasmic lipid droplets, and then incubated with TMAO. Treatment with TMAO was associated with changes in cell morphology, and substantially reduced the numbers of oil red-O-positive cells (Figure 4A). We confirmed that TMAO had no effect on adipocyte markers in ADSC under ADSC differentiation conditions, when adipocyte markers (adiponectin, PPAR- γ and perilipin) are significantly increased in ADSC with the adipocyte differentiation (Figures 4B and 4C). TMAO caused a marked reduction in adipocyte-specific gene expression while augmenting the expression of fibrotic genes (Figures 4C and 4D). Collectively, these results indicate that in distinct human mesenchymal cell populations TMAO promotes myofibroblast differentiation.

Profibrotic TMAO responses are mediated via PERK

A recent study identified a cellular receptor for TMAO in hepatocytes, where TMAO was shown to induce the expression of ER stress genes via the endoplasmic reticulum stress kinase (PERK, EIF2AK3) branch of the unfolded protein response (Chen et al., 2019). TMAO is reported to directly bind to PERK at physiologically relevant concentrations and to induce FoxO1 transcription factor, a key driver in metabolic syndrome (Chen et al., 2019). However, the mechanisms underlying the profibrotic effects of TMAO in mesenchymal cells are unknown. We sought to determine the role of PERK, which has not been directly implicated in fibrosis, in mediating mesenchymal cell TMAO responses. Incubation of confluent fibroblasts with TMAO induced a rapid and dose-dependent increase in PERK phosphorylation (Figure 5A). In parallel

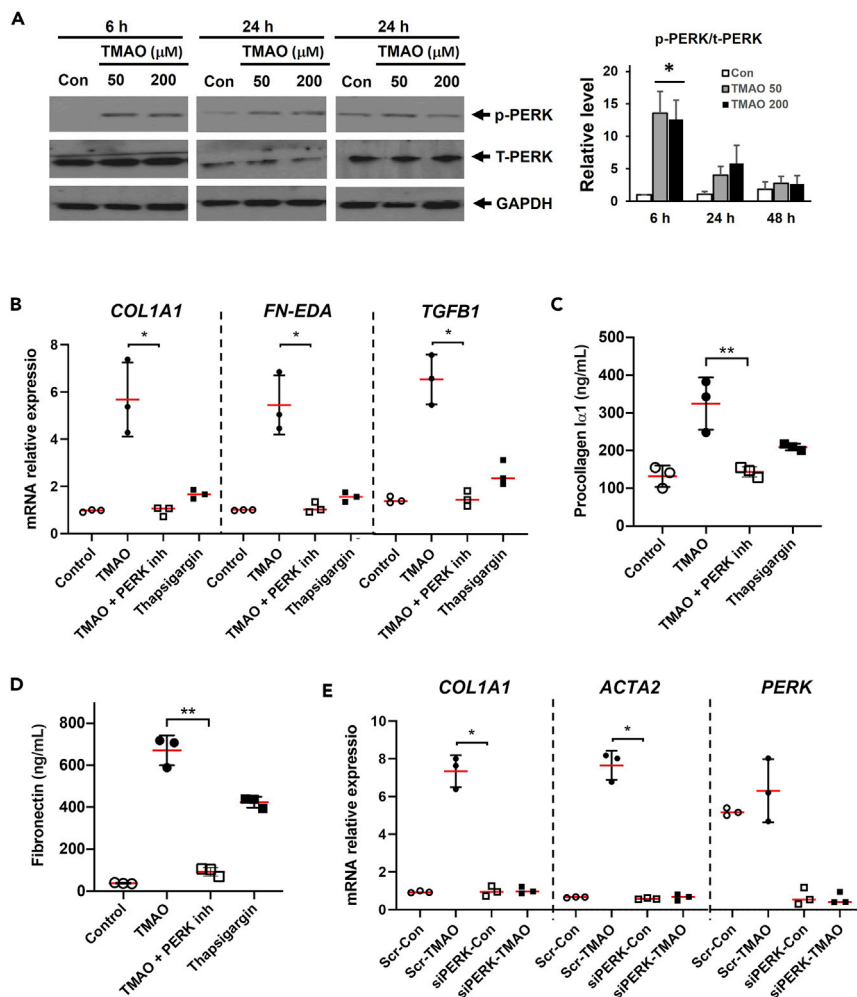


Figure 5. PERK is activated by TMAO to mediate fibrotic responses

(A) Confluent skin fibroblasts were incubated with TMAO for indicated periods, and whole cell lysates were subjected to immunoblot analysis. Representative images.

(B) Cultures were preincubated in media with GSK 2606414 (10 μM) for 6 h prior to TMAO (200 μM) or thapsigargin (0.25 μM) for 48 h, followed by qPCR. Results are means ± SEM of triplicate determination.

(C and D). Following 48 h incubation, media were harvested and assayed for secreted procollagen Iα1 and fibronectin-EDA. Results are means ± SD of three determinations. (*p < 0.05 versus controls; n = 3).

(E) Fibroblasts were transfected with PERK siRNA or scrambled control siRNA. After 72 h TMAO (200 μM) was added to the media for 48 h. Cultures were harvested and total RNA was subjected to qPCR. (*p < 0.05 versus control; n = 3).

experiments, the prototypic fibrotic stimulus TGF-β1 had no detectable effect on PERK activation. TMAO treatment induced comparable PERK activation in HMVECs that was accompanied by increased Foxo1 expression (Figure 6C). Next, we sought to explore the role of PERK in TMAO-driven endoMT using complementary pharmacological and genetic approaches. Blocking PERK activity using the selective inhibitor GSK 2606414 abrogated TMAO-dependent stimulation of *COL1A1*, *FN-EDA* and *TGFB1* mRNA expression and procollagen and fibronectin-EDA production (Figures 5B–5D). RNAi-mediated silencing of PERK in ECs had a comparable inhibitory effect on TMAO-mediated stimulation of *COL1A1* and *ACTA2* (Figure 5E) and other fibroblast markers while preventing suppression of VE-cadherin (CDH5) and PECAM-1 (CD31) (Figures 6A and 6B). Of note, the prototypic chemical ER stress inducer thapsigargin had no detectable effect on TMAO-induced fibrotic responses, suggesting that PERK-mediated TMAO responses were independent of ER stress. We next examined the effect of TMAO on endothelial cell migration using scratch-wound assays. Treatment of confluent HMVECs with TMAO (50 μM) significantly accelerated their migration over 72 h (Figure 6D). These profibrotic cellular responses to TMAO were prevented by PERK

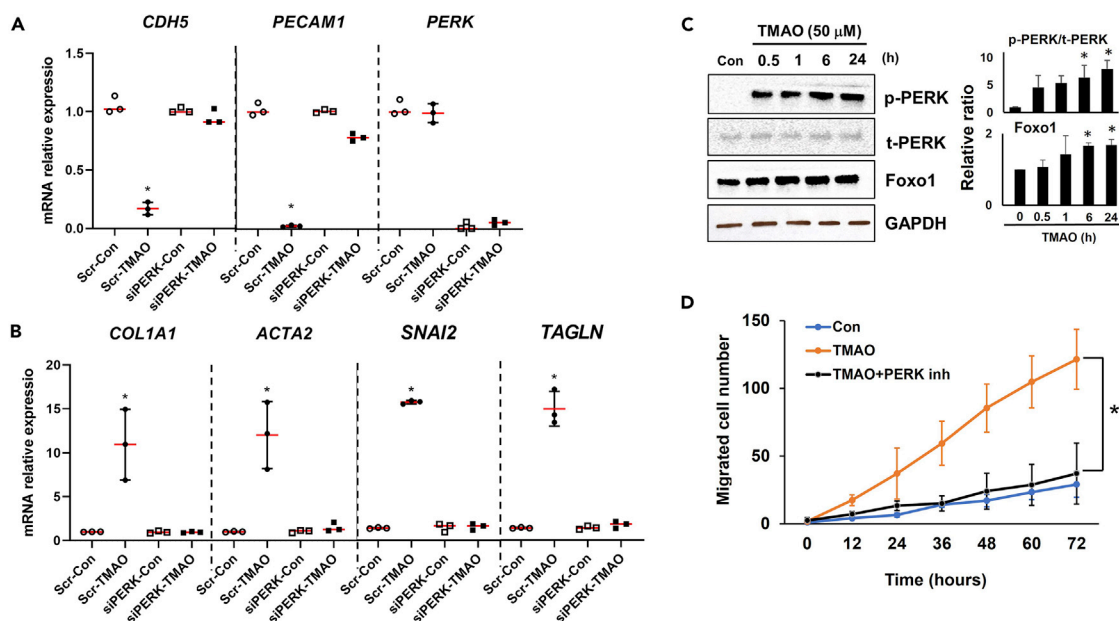


Figure 6. PERK deficiency attenuates TMAO-mediated EndoMT

Confluent HMVECs transfected with PERK siRNA or scrambled control siRNA were incubated in media with TMAO (50 μ M) for 72 h or indicated periods. (A and B) Total RNA was subjected to real-time qPCR. Result are means \pm SEM of triplicate determinations.

(C) Whole cell lysates were used for immunoblotting with antibodies to phospho-PERK, total PERK and Foxo1. Representative images.

(D) Scratch-wound assays. Confluent HMVECs were incubated in media with TMAO (50 μ M) and GSK 2606414 (10 μ M). Scratch wounds were then created and cell migration at 48 h was measured. Results are means \pm SD of three determinations. (* p < 0.05 versus control; n = 3).

inhibition. Together these results unambiguously implicate PERK in mediating the profibrotic effects of TMAO in mesenchymal cells.

The TMA-converting cellular enzyme FMO3 is expressed in fibroblasts and induced by TGF- β 1

Generation of TMAO from gut microbiome-derived TMA is catalyzed in the host by FMO3 (Krueger and Williams, 2005). Although FMO3 is known to be expressed primarily in hepatocytes (Xu et al., 2017), extra-hepatic expression of FMO3 has also been documented; however, its role remains poorly understood (Janmohamed et al., 2001; Schugar et al., 2017). The expression level of FMO3 and its enzymatic activity, combined with substrate availability, determine organismal TMAO homeostasis in health and disease (Brown and Hazen, 2015). The human *FMO3* gene promoter harbors a CCAAT/enhancer-binding protein β (C/EBP β) element that plays a key regulatory role, and its mutation strongly reduces *FMO3* expression, whereas in genetically engineered mice, FMO3 expression correlates with TMAO levels (Esposito et al., 2014; Shih et al., 2019). Little is known regarding the expression and regulation of FMO3 in fibrotic diseases. A query of public transcriptome datasets (Figure 7A) revealed significantly upregulated FMO3 mRNA expression in human skin organ cultures treated with TGF- β 1 (Watanabe et al., 2019). Similarly, we found that in both explanted skin fibroblasts and HMVECs, TGF- β 1 augmented FMO3 expression, while levels of FMO1 remained unchanged (Figures 7B and 7C).

FMO3 expression is elevated in SSc skin cell populations *in vivo* and *in vitro*

We next queried published and unpublished skin transcriptome datasets to evaluate FMO3 expression in SSc (Table 1). Skin fibroblasts that were freshly isolated and flow-sorted from skin biopsies of early-stage SSc patients (Chadli et al., 2019) showed >4-fold higher levels of FMO3 mRNA compared to control fibroblasts (p < 0.05). Analysis of multiple transcriptome datasets (summarized in Table 1) showed elevated expression of FMO3 in SSc skin biopsies consistent across five independent patient cohorts, with -fold increase ranging from 1.69 to 4.29. As an example, querying a transcriptome dataset of skin biopsies from a cohort of SSc patients with early-stage disease [Prospective Registry for Early Systemic Sclerosis (PRESS)] showed that FMO3 expression was 1.78-fold higher compared to healthy controls [GEO: GSE130955] (Skaug et al., 2020). Skin biopsies from the Genetics versus Environment in Scleroderma Outcome Study

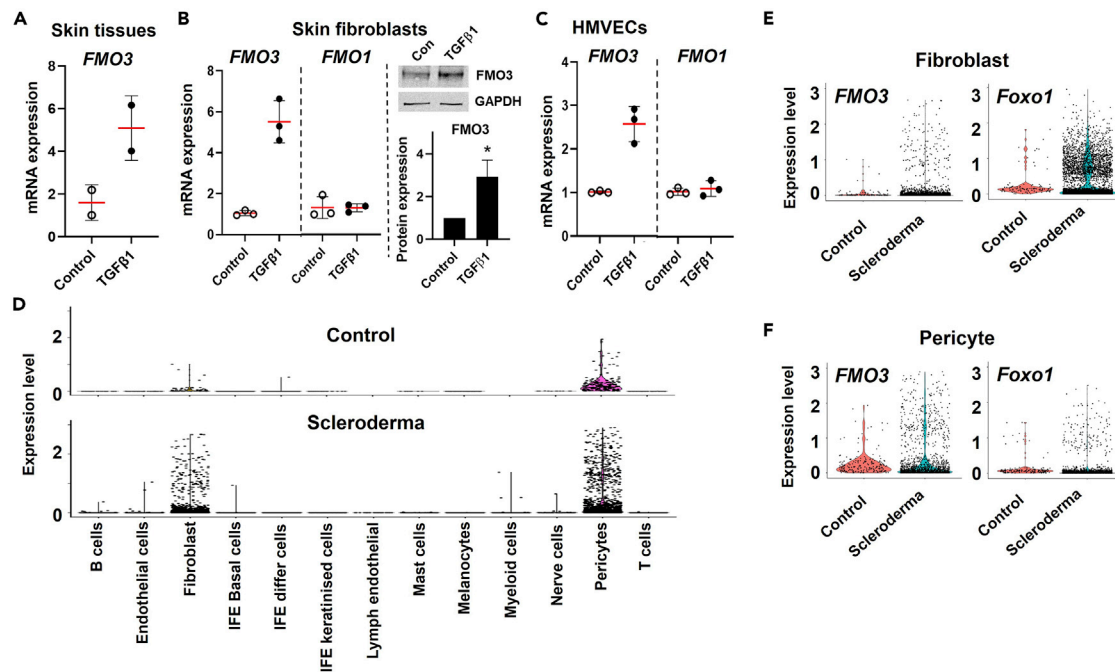


Figure 7. Inducible expression of FMO3 in skin and elevated levels in SSc

(A). FMO3 mRNA is induced by TGF- β 1 (10 ng/mL) treatment for 48 h of human skin explants (GSE109350).

(B and C) Confluent dermal fibroblasts (B) or HMVECs (C) were incubated with TGF- β 1 (5 ng/mL), and following 48 h incubation, whole cell lysates were analyzed by immunoblotting (B, right panel), and total RNA was isolated and subjected to real-time qPCR; results are means \pm SD of three determinations (left panel).

(D) Skin biopsies from healthy controls (n = 2) and SSc patients (n = 6) were subjected to scRNA-seq analysis. Single-cell gene expression levels for FMO3 across cell clusters.

(E and F) Relative FMO3 and Foxo1 expression in fibroblast and pericyte subpopulations in SSc and healthy control biopsies.

(GENISOS) cohort of 59 SSc patients showed a 2.71-fold increase in FMO3 expression compared to controls [GEO: GSE47162] (Assassi et al., 2013).

By bulk RNA sequencing, we found elevated expression of FMO3 in SSc skin biopsies. To further investigate FMO3 expression in the skin, we performed single-cell RNA-seq analysis on skin biopsies from a distinct cohort of SSc patients and healthy controls. Unsupervised clustering identified distinct clusters with their putative cellular identities based on gene expression signatures associated with the corresponding clusters (Tabib et al., 2021). FMO3 gene expression in SSc biopsies mapped primarily to fibroblasts and pericytes (Figures 7D–7F). Focused analysis identified seven fibroblast subpopulations in the skin, with the highest proportion of FMO3+ cells in CLDN1+ fibroblasts (Figure S4).

To detect and measure FMO3 protein in the skin, we used immunolabeling of biopsies from SSc patients and healthy controls (Table 2) using anti-FMO3 antibodies. The numbers of FMO3-immunopositive dermal cells (predominantly associated with vasculature, as discussed in the following sections) were significantly elevated in SSc biopsies (Figures 8A and 8B). Vascular FMO3 in these biopsies varied from patchy to extensive and highlighted the outer vessel walls. In addition, FMO3 was detected in perineurial cells (focal to extensive), occasional deep dermal fibroblastic cells, and in subcutaneous adipocytes. In healthy control skin biopsies, vascular expression of FMO3 was limited, and perineurial immunostaining was negative. Subcutaneous tissue was not consistently present in healthy controls, precluding rigorous comparisons at this tissue plane. We next examined the expression of FMO3 in isolated fibroblasts explanted from SSc skin biopsies (Table 3). As shown in Figure 8B, FMO3 was detectable in fibroblasts in culture, and levels were consistently elevated in SSc compared to healthy control fibroblasts studied in parallel. These results are in agreement with previous reports showing elevated FMO3 mRNA levels in freshly isolated SSc skin fibroblasts. Importantly, we found that intracellular Type I collagen levels in SSc fibroblasts were associated with FMO3 expression. Comparable results were seen in fibroblasts immunolabeled using procollagen I

Table 1. FMO expression in SSc skin: transcriptome datasets

Source	Tissue/Cell	Disease	Transcriptome type	FC	p value	GEO ID	References
Gardet	Skin fibroblast	Early diffuse SSc	RNA microarray	4.29	1.91E-06	N.A.	Scientific reports 2019
Lafyatis	Skin (Biopsy)	DcSSc	Bulk RNA seq	1.69	6.96e-03	GSE95065	Unpublished
Skaug/Assassi	Skin (Biopsy)	Early SSc	Bulk RNA seq	1.78	2.07E-12	GSE130955	Ann Rheum Dis 2020
Assassi	Skin (Biopsy)	ILD in SSc	Bulk RNA seq	2.71	1.19E-09	GSE47162	Arthritis Rheum 2013
Gudjonsson	Skin (Biopsy)	SSc	Bulk RNA seq	3.82	4.51E-07	N.A.	Unpublished

* SSc: systemic sclerosis.

* dc: diffuse cutaneous.

* ILD: interstitial lung disease.

* FC: fold change.

antibodies. Importantly, SSc fibroblasts showed increased phospho-PERK levels, indicative of constitutive cell-autonomous activated PERK pathway signaling (Figure 8C). These results indicate that FMO3, the intracellular enzyme responsible for converting gut-derived TMA to TMAO in the host, is present in mesenchymal cells in the skin and its expression is upregulated by TGF- β 1. In SSc, skin biopsies, significant upregulation of FMO3 was observed in multiple stromal cell populations, including fibroblasts that show constitutive FMO3 overexpression associated with PERK activation *ex vivo*. Together, these observations suggest that cell-autonomous upregulation of FMO3 in SSc fibroblasts might contribute to their elevated collagen production underlying fibrosis.

DISCUSSION

The etiology of SSc involves a complex interplay of heritable and environmental factors (Allanore et al., 2015). However, the mechanisms linking SSc genetic risk variants and environmental exposures with the hallmark microvascular and fibrotic processes underlying the clinical manifestations of SSc are unknown. Here, we demonstrate that TMAO, generated in the host via FMO3 from TMA generated in the gut via microbial metabolism, drives myofibroblast reprogramming of various mesenchymal progenitor cells. These fibrotic responses, including endothelial cell transition to myofibroblasts, are mediated via activation of PERK. Moreover, we demonstrate that expression of FMO3 is elevated in mesenchymal cell populations in SSc skin biopsies, and in isolated SSc skin fibroblasts. Thus, the TMA-FMO3-TMAO axis might represent a metaorganismal pathway underlying microvascular remodeling and tissue fibrosis in SSc.

Human and animal studies have demonstrated that elevated TMAO is associated with vascular injury and fibrosis in the heart, kidneys, and other organs (Gupta et al., 2020; Li et al., 2019; Organ et al., 2016; Tang et al., 2013; Wang et al., 2015; Zhu et al., 2016). However, the pathogenic role, mechanism of action, and clinical implications of elevated TMAO in the context of SSc have never been studied. Here, we demonstrate that TMAO directly stimulates fibrotic responses in a variety of skin-resident mesenchymal cell populations via activation of its putative cellular receptor PERK. Our results show that TMAO induced endoMT in dermal microvascular endothelial cells and promoted fibroblast differentiation in adipocyte-derived stem cells.

A hallmark of fibrosis in the skin and other affected organs is accumulation of ECM and activated myofibroblasts (Bonnans et al., 2014; Gibb et al., 2020). The origins of the myofibroblasts in fibrosis are not fully understood (Hinz et al., 2012; Pakshir and Hinz, 2018). Our results show that in microvascular endothelial cells TMAO directly induces endoMT, with downregulation of endothelial markers. Adipocytes are mesenchymal-derived cells which have important endocrine and paracrine effects mediated through adipokines (Zwick et al., 2018). Skin fibrosis has been linked to loss of dermal adipose tissue (Marangoni et al., 2015). We and others have described AMT as a process whereby differentiated white adipocytes acquire a myofibroblast phenotype when cultured in the presence of profibrotic stimuli (Marangoni et al., 2015). Our present results indicate that treatment with TMAO substantially attenuated adipocytic differentiation of adipocytes, with downregulation PPAR- γ , perilipin, FABP4, and concomitant induction of fibrotic genes (type I collagen, α -SMA, etc.) indicating transition to a myofibroblast phenotype.

The gut microbiome plays important roles in human health and disease, and altered microbiome has been linked with SSc (Clemente et al., 2012; Manor et al., 2020; Nagatomo and Tang, 2015; Witkowski et al.,

Table 2. Demographic and clinical features of subjects (skin biopsies used for IHC analysis)

Identifier	Age (years)	Sex	Race	Diagnosis	Disease duration	MRS
SPARC_Normal 04	26	Female	Hispanic	Control	N/A	N/A
SPARC_Normal 05	26	Male	White	Control	N/A	N/A
SPARC_Normal 06	26	Female	White	Control	N/A	N/A
SPARC_Normal 07	29	Male	African American	Control	N/A	N/A
SPARC_Normal 13	57	Female	White	Control	N/A	N/A
SPARC_Normal 14	50	Male	White	Control	N/A	N/A
SPARC_Normal 15	32	Female	White	Control	N/A	N/A
SPARC_Normal 16	22	Female	White	Control	N/A	N/A
SPARC_SSc 29	50	Female	White	dcSSc	20	33
SPARC_SSc 32	42	Female	White	dcSSc	63	23
SPARC_SSc 33	43	Male	White	dcSSc	15	13
SPARC_SSc 37	63	Female	White	dcSSc	13	34
SPARC_SSc 41	43	Female	White	dcSSc	16	13
SPARC_SSc 42	62	Male	White	dcSSc	15	35
SPARC_SSc 43	55	Female	African American	dcSSc	11	27

*dcSSc, diffuse cutaneous SSc; MRSS, modified Rodnan skin score (max. 51).

2020). The gut microbiome-derived metabolite TMAO has been shown to be atherogenic in mice and associated with major adverse cardiovascular events in humans (Witkowski et al., 2020). In addition, elevated TMAO is implicated in cardiac and renal fibrosis in mice (Gupta et al., 2020; Zhang et al., 2021). Although fibroblast activation elicited by TGF- β 1, chemokines and other extracellular cues is recognized as an essential early step in the development of fibrosis, an association between TMAO and myofibroblast differentiation has not been previously demonstrated (Allanore et al., 2015; Angiolilli et al., 2018; Distler et al., 2019; Sobolewski et al., 2019). A recent study showed that TMAO binds to PERK and selectively activates the PERK branch of the unfolded protein response (UPR), implicating PERK in TMAO-dependent modulation of glucose metabolism (Chen et al., 2019). PERK and its downstream targets have been implicated, and their inhibition has beneficial effects, in diabetes, atherosclerosis, and kidney disease (Chiang et al., 2011; Choi et al., 2016; Masuda et al., 2013; Onat et al., 2019). We found that TMAO significantly increased profibrotic gene expression in human foreskin fibroblasts, and these effects are mediated by activation of cellular PERK (Kumashiro et al., 2011). Although TMAO treatment in mesenchymal cells was associated with increased TGF- β 1 production, the profibrotic effects of TMAO are unlikely to be mediated via endogenous TGF- β 1, because in contrast to exogenous TGF- β 1, TMAO failed to elicit activation of Smad2. Treatment of fibroblasts with TMA—the gut-derived metabolic precursor of TMAO—itself induced activation of PERK and modest fibrotic responses but only at relatively high concentrations, possibly indicating conversion to TMAO within FMO3-expressing fibroblasts.

Elevated TMAO levels have a strong association with cardiac and renal tubulointerstitial fibrosis and contribute to heart failure and chronic kidney disease (Chen et al., 2017; Gupta et al., 2020; Li et al., 2019; Tang et al., 2015; Zhang et al., 2021). TMAO is generated from dietary factors, such as choline, which are converted by the gut microbes to TMA, which is in turn converted to TMAO by host FMO3 (Koeth et al., 2013; Romano et al., 2017; Wang et al., 2011). *Fmo3* gene expression is reduced in hepatic oxidative stress liver injury models (Rudraiah et al., 2014). Numerous roles for FMO3 itself in health and disease have been suggested in studies using mice. Knockdown of FMO3 in low-density lipoprotein receptor-knockout mice uncovered a role for FMO3 in glucose and lipid homeostasis (Shih et al., 2015). Hepatic and extrahepatic expression of FMO3 is variable and has been shown to be altered in a variety of conditions, including insulin resistance (Miao et al., 2015). Suggested roles for FMO3 include involvement in cholesterol metabolism and reverse cholesterol transport (Barrett and Kwan, 1985). Our results demonstrate that TGF- β 1 induces FMO3 expression in human foreskin fibroblasts. Individuals harboring nonsense FMO3 mutations exhibit abnormally low levels of trimethylamine N-oxygenation (Shimizu et al., 2015). Furthermore, previous single-cell RNA-seq studies identified FMO expression in dermal fibroblasts (Apostolidis et al., 2018). Of potential significance, previous studies using scRNA-seq of the lung indicated that FMO3 expression was

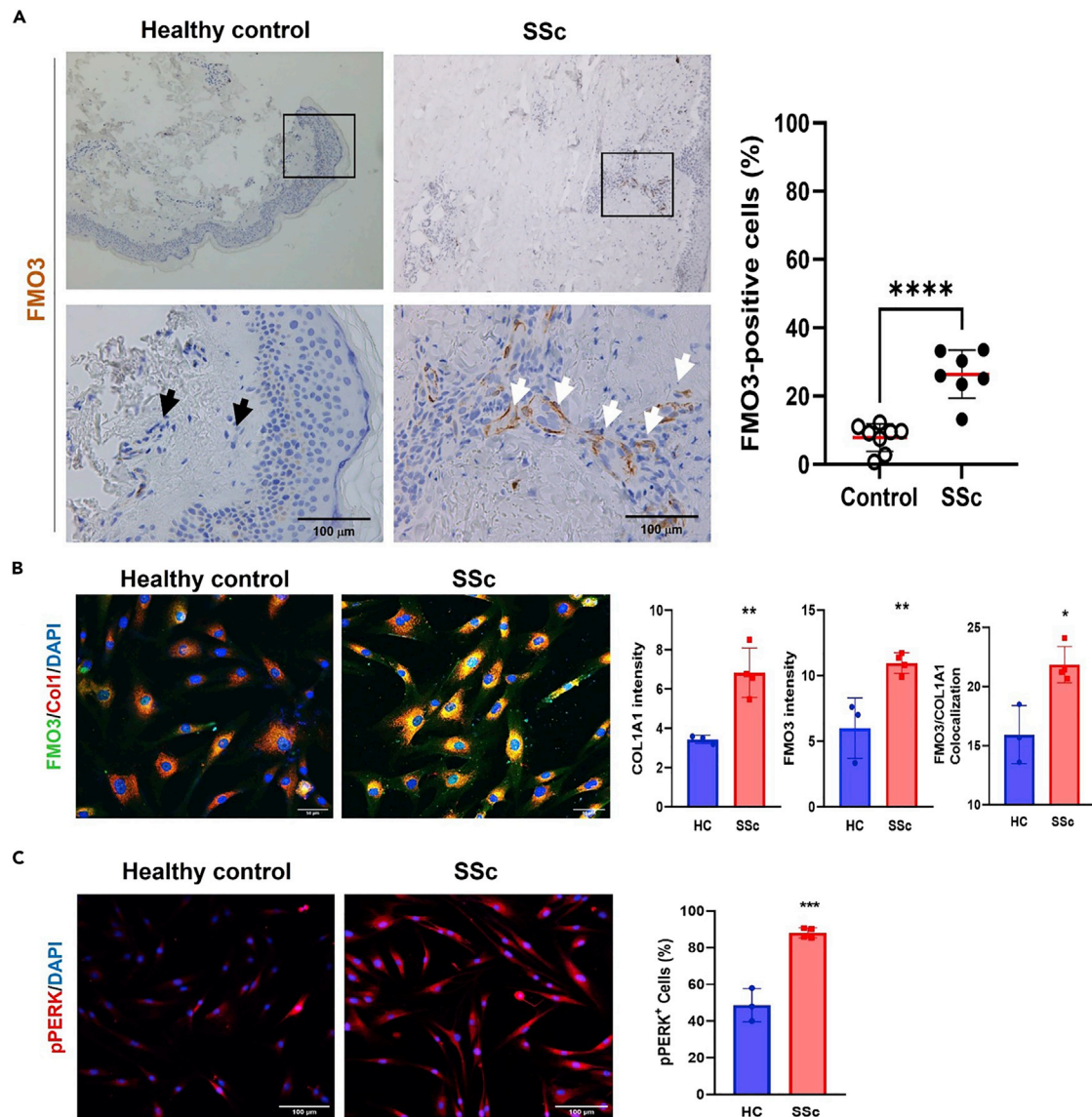


Figure 8. TMAO-generating FMO3 is significantly elevated in SSc skin biopsies and isolated fibroblasts

(A) Skin biopsies from healthy controls (n = 8) and SSc patients (n = 7) were immunolabeled with anti-FMO3 antibodies. Left panels, representative images. White arrows indicate FMO3⁺ cells around the outer wall of dermal vessels. Bars = 100 μ m. Right panel, quantitation of FMO3⁺ cells in the dermis; horizontal bars, means \pm SEM (*p < 0.0001). Clinical information shown in [Table 2](#).

(B and C) Confluent skin fibroblasts explanted from SSc (n = 4) and healthy adult control (HC; n = 3) biopsies were immunolabeled using antibodies to FMO3, Type I collagen and p-PERK. Nuclei were identified by DAPI staining. Representative confocal images. Bar graphs showing immunofluorescence intensities are means \pm SEM.

elevated in fibroblasts and other stromal cell populations in IPF (IPF Cell Atlas). Remarkably, fibroblasts from patients with early-stage SSc show elevated FMO3 levels compared to matched control fibroblasts ([Chadli et al., 2019](#)). In addition, published and unpublished human studies show that FMO3 levels are increased in skin biopsies from SSc patients ([Table 1](#)). Here, we identify fibroblasts and pericytes as the predominant FMO3-overexpressing cells in SSc skin biopsies, and further map FMO3 expression to the CLDN1⁺ fibroblast subpopulation. Further studies will be needed to characterize these fibroblasts and determine their specific roles in the pathogenesis of SSc.

Together, the observations presented here indicate that TMAO exerts potent profibrotic effects mediated via PERK-dependent myfibroblast differentiation of skin-resident mesenchymal precursor cells

Table 3. Demographic and clinical features of subjects of explanted skin fibroblasts used for immunolabeling

SSc biopsy	Subject Age (yrs)	Sex	Diagnosis
SSc 21	49	F	dcSSc
SSc 22	51	F	dcSSc
SSc 24	69	F	dcSSc
SSc 25	45	F	dcSSc

*dcSSc, diffuse cutaneous SSc.

(fibroblasts, adipocytes, and endothelial cells). The TMAO-generating enzyme FMO3 is expressed in the skin and maps to fibroblasts and pericytes. FMO3 expression is significantly elevated in SSc skin and in isolated SSc fibroblasts, where it is associated with constitutive PERK activation and increased collagen production. Elevated FMO3 expression and/or activity could conceivably contribute to enhanced TMAO generation and consequent myofibroblast accumulation and ECM remodeling systemically or in a tissue-restricted manner. This new paradigm potentially integrates dietary factors with host TMAO metabolism via genetic variants of FMO3 and/or its modified expression in a meta-organismal pathway that drives disease and represents a new potential target for pharmacological disease-modifying therapy for SSc.

Limitations of the study

There are some limitations of our study. Our present findings demonstrating a profibrotic effect of TMAO are based on cellular assays. The observed impact of TMAO on promoting myofibroblast transition across fibroblasts, microvascular endothelial cells, and preadipocytes, notwithstanding whether TMAO exposure will promote a fibrotic phenotype in animals still remains to be determined. Moreover, although the detection of FMO3 in skin fibroblasts is interesting, in view of its well-known localization in the liver, we have not established in the present work if fibroblast FMO3 shows enzymatic activity and is capable of catabolizing TMA to TMAO comparable to liver FMO3. In addition, the cellular mechanisms responsible for fibrotic responses downstream of activated PERK in TMAO-treated mesenchymal cells, including specific chromatin modifications, require detailed elucidation.

STAR★METHODS

Detailed methods are provided in the online version of this paper and include the following:

- KEY RESOURCES TABLE
- RESOURCE AVAILABILITY
 - Lead contact
 - Materials availability
 - Data and code availability
- EXPERIMENTAL MODEL AND SUBJECT DETAILS
 - Cell culture and reagents
 - Quantitative real-time PCR (qPCR)
 - Measurement of collagen, fibronectin and TGF-β1 secretion
 - Immunofluorescence confocal microscopy
 - Immunoblot analysis
 - RNA sequencing
 - Cell migration assays
 - ADSC differentiation assays
 - Single-cell RNA-sequencing (scRNA-seq) analysis in skin biopsies
 - Skin histology and immunochemistry
 - Quantification of histone H3 modifications
- QUANTIFICATION AND STATISTICAL ANALYSIS

SUPPLEMENTAL INFORMATION

Supplemental information can be found online at <https://doi.org/10.1016/j.isci.2022.104669>.

ACKNOWLEDGMENT

Supported by NIH grants AR076821 (to John Varga), K08HL130601 (to Karen Ho) and 5R21AG060211 (to Seok-Jo Kim). We thank the Rogel Cancer Center Tissue and Molecular Pathology Shared Resource (supported by NIH CA04659229) for technical assistance.

AUTHOR CONTRIBUTIONS

J.V. supervised the study and wrote the manuscript. S.K. and S.B. designed and wrote the manuscript. P.V. and Q.W. generated and analyzed data. J.G. analyzed the data and developed the computational tools. S.H. provided clinical insights. P-S.T. provided technical support. D.K. and L.T. developed the computational tools. N.G. provided technical support. K.H. designed the study and provided clinical insights.

DECLARATION OF INTERESTS

Dr Hazen is named as coinventor on pending and issued patents held by the Cleveland Clinic relating to cardiovascular diagnostics or therapeutics, and reports having the right to receive royalty payment for inventions or discoveries related to cardiovascular diagnostics or therapeutics from Cleveland Heart Laboratory Inc, Quest Diagnostics and Procter & Gamble. Dr Hazen also reports having been paid as a consultant for Procter & Gamble, and receiving research funds from AstraZeneca, Procter & Gamble, Pfizer Inc, and Roche Diagnostics. Other authors declare no competing interests.

INCLUSION AND DIVERSITY

We worked to ensure gender balance in the recruitment of human subjects. We worked to ensure ethnic or other types of diversity in the recruitment of human subjects. We worked to ensure that the study questionnaires were prepared in an inclusive way. While citing references scientifically relevant for this work, we also actively worked to promote gender balance in our reference list.

Received: August 23, 2021

Revised: March 24, 2022

Accepted: June 21, 2022

Published: July 15, 2022

REFERENCES

- Allanore, Y., Simms, R., Distler, O., Trojanowska, M., Pope, J., Denton, C.P., and Varga, J. (2015). Systemic sclerosis. *Nat. Rev. Dis. Primers* 1, 15002. <https://doi.org/10.1038/nrdp.2015.2>.
- Anders, S., Pyl, P.T., and Huber, W. (2015). HTSeq—a Python framework to work with high-throughput sequencing data. *Bioinformatics* 31, 166–169. <https://doi.org/10.1093/bioinformatics/btu638>.
- Angiolilli, C., Marut, W., van der Kroef, M., Chouri, E., Reedquist, K.A., and Radstake, T.R.D.J. (2018). New insights into the genetics and epigenetics of systemic sclerosis. *Nat. Rev. Rheumatol.* 14, 657–673. <https://doi.org/10.1038/s41584-018-0099-0>.
- Apostolidis, S.A., Stifano, G., Tabib, T., Rice, L.M., Morse, C.M., Kahaleh, B., and Lafyatis, R. (2018). Single cell RNA sequencing identifies HSPG2 and APLNR as markers of endothelial cell injury in systemic sclerosis skin. *Front. Immunol.* 9, 2191. <https://doi.org/10.3389/fimmu.2018.02191>.
- Assassi, S., Wu, M., Tan, F.K., Chang, J., Graham, T.A., Furst, D.E., Khanna, D., Charles, J., Ferguson, E.C., Feghali-Bostwick, C., and Mayes, M.D. (2013). Skin gene expression correlates of severity of interstitial lung disease in systemic sclerosis. *Arthritis Rheum.* 65, 2917–2927. <https://doi.org/10.1002/art.38101>.
- Barrett, E.L., and Kwan, H.S. (1985). Bacterial reduction of trimethylamine oxide. *Annu. Rev. Microbiol.* 39, 131–149. <https://doi.org/10.1146/annurev.mi.39.100185.001023>.
- Belkaid, Y., and Hand, T.W. (2014). Role of the microbiota in immunity and inflammation. *Cell* 157, 121–141. <https://doi.org/10.1016/j.cell.2014.03.011>.
- Bennett, B.J., de Aguiar Vallim, T.Q., Wang, Z., Shih, D.M., Meng, Y., Gregory, J., Allayee, H., Lee, R., Graham, M., Crooke, R., et al. (2013). Trimethylamine-N-oxide, a metabolite associated with atherosclerosis, exhibits complex genetic and dietary regulation. *Cell Metabol.* 17, 49–60. <https://doi.org/10.1016/j.cmet.2012.12.011>.
- Bhattacharyya, S., Wei, J., and Varga, J. (2012). Understanding fibrosis in systemic sclerosis: shifting paradigms, emerging opportunities. *Nat. Rev. Rheumatol.* 8, 42–54. <https://doi.org/10.1038/nrrheum.2011.149>.
- Bischoff, J. (2019). Endothelial-to-mesenchymal transition: purposeful versus maladaptive differentiation. *Circ. Res.* 124, 1163–1165. <https://doi.org/10.1161/circresaha.119.314813>.
- Bonnans, C., Chou, J., and Werb, Z. (2014). Remodelling the extracellular matrix in development and disease. *Nat. Rev. Mol. Cell Biol.* 15, 786–801. <https://doi.org/10.1038/nrm3904>.
- Brown, J.M., and Hazen, S.L. (2015). The gut microbial endocrine organ: bacterially derived signals driving cardiometabolic diseases. *Annu. Rev. Med.* 66, 343–359. <https://doi.org/10.1146/annurev-med-060513-093205>.
- Butler, A., Hoffman, P., Smibert, P., Papalexis, E., and Satija, R. (2018). Integrating single-cell transcriptomic data across different conditions, technologies, and species. *Nat. Biotechnol.* 36, 411–420. <https://doi.org/10.1038/nbt.4096>.
- Chadli, L., Soththwes, B., Li, K., Andersen, S.N., Cahir-McFarland, E., Cheung, M., Cullen, P., Dorjée, A., de Vries-Bouwstra, J.K., Huizinga, T.W.J., et al. (2019). Identification of regulators of the myofibroblast phenotype of primary dermal fibroblasts from early diffuse systemic sclerosis patients. *Sci. Rep.* 9, 4521. <https://doi.org/10.1038/s41598-019-41153-w>.
- Chen, K., Zheng, X., Feng, M., Li, D., and Zhang, H. (2017). Gut microbiota-dependent metabolite trimethylamine N-oxide contributes to cardiac dysfunction in western diet-induced obese mice. *Front. Physiol.* 8, 139. <https://doi.org/10.3389/fphys.2017.00139>.
- Chen, S., Henderson, A., Petriello, M.C., Romano, K.A., Gearing, M., Miao, J., Schell, M., Sandoval-

- Espinola, W.J., Tao, J., Sha, B., et al. (2019). Trimethylamine N-oxide binds and activates PERK to promote metabolic dysfunction. *Cell Metabol.* 30, 1141–1151.e5. <https://doi.org/10.1016/j.cmet.2019.08.021>.
- Chiang, C.-K., Hsu, S.-P., Wu, C.-T., Huang, J.-W., Cheng, H.-T., Chang, Y.-W., Hung, K.-Y., Wu, K.-D., and Liu, S.-H. (2011). Endoplasmic reticulum stress implicated in the development of renal fibrosis. *Mol. Med.* 17, 1295–1305. <https://doi.org/10.2119/molmed.2011.00131>.
- Choi, S.K., Lim, M., Yeon, S.I., and Lee, Y.H. (2016). Inhibition of endoplasmic reticulum stress improves coronary artery function in type 2 diabetic mice. *Exp. Physiol.* 101, 768–777. <https://doi.org/10.1113/ep085508>.
- Clemente, J.C., Ursell, L.K., Parfrey, L.W., and Knight, R. (2012). The impact of the gut microbiota on human health: an integrative view. *Cell* 148, 1258–1270. <https://doi.org/10.1016/j.cell.2012.01.035>.
- Denton, C.P., and Khanna, D. (2017). Systemic sclerosis. *Lancet* 390, 1685–1699. [https://doi.org/10.1016/s0140-6736\(17\)30933-9](https://doi.org/10.1016/s0140-6736(17)30933-9).
- Di Benedetto, P., Ruscitti, P., Berardicurti, O., Vomero, M., Navarini, L., Dolo, V., Cipriani, P., and Giacomelli, R. (2021). Endothelial-to-mesenchymal transition in systemic sclerosis. *Clin. Exp. Immunol.* 205, 12–27. <https://doi.org/10.1111/cei.13599>.
- Distler, J.H.W., Györfi, A.-H., Ramanujam, M., Whitfield, M.L., Königshoff, M., and Lafyatis, R. (2019). Shared and distinct mechanisms of fibrosis. *Nat. Rev. Rheumatol.* 15, 705–730. <https://doi.org/10.1038/s41584-019-0322-7>.
- Esposito, T., Varriale, B., D'Angelo, R., Amato, A., and Sidoti, A. (2014). Regulation of flavin-containing mono-oxygenase (Fmo3) gene expression by steroids in mice and humans. *Horm. Mol. Biol. Clin. Invest.* 20, 99–109. <https://doi.org/10.1515/hmbci-2014-0012>.
- Fang, F., Liu, L., Yang, Y., Tamaki, Z., Wei, J., Marangoni, R.G., Bhattacharyya, S., Sumner, R.S., Ye, B., and Varga, J. (2012). The adipokine adiponectin has potent anti-fibrotic effects mediated via adenosine monophosphate-activated protein kinase: novel target for fibrosis therapy. *Arthritis Res. Ther.* 14, R229. <https://doi.org/10.1186/ar4070>.
- Gibb, A.A., Lazaropoulos, M.P., and Elrod, J.W. (2020). Myofibroblasts and fibrosis: mitochondrial and metabolic control of cellular differentiation. *Circ. Res.* 127, 427–447. <https://doi.org/10.1161/circresaha.120.316958>.
- Gupta, N., Buffa, J.A., Roberts, A.B., Sangwan, N., Skye, S.M., Li, L., Ho, K.J., Varga, J., DiDonato, J.A., Tang, W.W., and Hazen, S.L. (2020). Targeted inhibition of gut microbial trimethylamine N-oxide production reduces renal tubulointerstitial fibrosis and functional impairment in a murine model of chronic kidney disease. *Arterioscler. Thromb. Vasc. Biol.* 40, 1239–1255. <https://doi.org/10.1161/atvbaha.120.314139>.
- Hinz, B., and Lagares, D. (2020). Evasion of apoptosis by myofibroblasts: a hallmark of fibrotic diseases. *Nat. Rev. Rheumatol.* 16, 11–31. <https://doi.org/10.1038/s41584-019-0324-5>.
- Hinz, B., Phan, S.H., Thannickal, V.J., Prunotto, M., Desmoulière, A., Varga, J., De Wever, O., Mareel, M., and Gabbiani, G. (2012). Recent developments in myofibroblast biology: paradigms for connective tissue remodeling. *Am. J. Pathol.* 180, 1340–1355. <https://doi.org/10.1016/j.ajpath.2012.02.004>.
- Janeiro, M.H., Ramírez, M.J., Milagro, F.I., Martínez, J.A., and Solas, M. (2018). Implication of trimethylamine N-oxide (TMAO) in disease: potential biomarker or new therapeutic target. *Nutrients* 10, 1398. <https://doi.org/10.3390/nu10101398>.
- Janmohamed, A., Dolphin, C.T., Phillips, I.R., and Shephard, E.A. (2001). Quantification and cellular localization of expression in human skin of genes encoding flavin-containing monooxygenases and cytochromes P450 2AAbbreviations: FMO, flavin-containing monooxygenase; CYP, cytochrome P450; KGM, keratinocyte growth medium; DMEM, Dulbecco's modified Eagle's medium. *Biochem. Pharmacol.* 62, 777–786. [https://doi.org/10.1016/s0006-2952\(01\)00718-3](https://doi.org/10.1016/s0006-2952(01)00718-3).
- Jimenez, S.A. (2013). Role of endothelial to mesenchymal transition in the pathogenesis of the vascular alterations in systemic sclerosis. *ISRN Rheumatol.* 2013, 835948. <https://doi.org/10.1155/2013/835948>.
- Koeth, R.A., Wang, Z., Levison, B.S., Buffa, J.A., Org, E., Sheehy, B.T., Britt, E.B., Fu, X., Wu, Y., Li, L., et al. (2013). Intestinal microbiota metabolism of L-carnitine, a nutrient in red meat, promotes atherosclerosis. *Nat. Med.* 19, 576–585. <https://doi.org/10.1038/nm.3145>.
- Krueger, S.K., and Williams, D.E. (2005). Mammalian flavin-containing monooxygenases: structure/function, genetic polymorphisms and role in drug metabolism. *Pharmacol. Ther.* 106, 357–387. <https://doi.org/10.1016/j.pharmthera.2005.01.001>.
- Kumashiro, N., Erion, D.M., Zhang, D., Kahn, M., Beddow, S.A., Chu, X., Still, C.D., Gerhard, G.S., Han, X., Dziura, J., et al. (2011). Cellular mechanism of insulin resistance in nonalcoholic fatty liver disease. *Proc. Natl. Acad. Sci. USA* 108, 16381–16385. <https://doi.org/10.1073/pnas.1113359108>.
- Li, B., Tsoi, L.C., Swindell, W.R., Gudjonsson, J.E., Tejasvi, T., Johnston, A., Ding, J., Stuart, P.E., Xing, X., Kochkodan, J.J., et al. (2014). Transcriptome analysis of psoriasis in a large case–control sample: RNA-seq provides insights into disease mechanisms. *J. Invest. Dermatol.* 134, 1828–1838. <https://doi.org/10.1038/jid.2014.28>.
- Li, X., Geng, J., Zhao, J., Ni, Q., Zhao, C., Zheng, Y., Chen, X., and Wang, L. (2019). Trimethylamine N-oxide exacerbates cardiac fibrosis via activating the NLRP3 inflammasome. *Front. Physiol.* 10, 866. <https://doi.org/10.3389/fphys.2019.00866>.
- Love, M.I., Huber, W., and Anders, S. (2014). Moderated estimation of fold change and dispersion for RNA-seq data with DESeq2. *Genome Biol.* 15, 550. <https://doi.org/10.1186/s13059-014-0550-8>.
- Manetti, M., Romano, E., Rosa, I., Guiducci, S., Bellando-Randone, S., De Paulis, A., Ibbamanneschi, L., and Matucci-Cerinic, M. (2017). Endothelial-to-mesenchymal transition contributes to endothelial dysfunction and dermal fibrosis in systemic sclerosis. *Ann. Rheum. Dis.* 76, 924–934. <https://doi.org/10.1136/annrheumdis-2016-210229>.
- Manor, O., Dai, C.L., Kornilov, S.A., Smith, B., Price, N.D., Lovejoy, J.C., Gibbons, S.M., and Magis, A.T. (2020). Health and disease markers correlate with gut microbiome composition across thousands of people. *Nat. Commun.* 11, 5206–5212. <https://doi.org/10.1038/s41467-020-18871-1>.
- Marangoni, R.G., Korman, B.D., Wei, J., Wood, T.A., Graham, L.V., Whitfield, M.L., Scherer, P.E., Tourtellotte, W.G., and Varga, J. (2015). Myofibroblasts in murine cutaneous fibrosis originate from adiponectin-positive intradermal progenitors. *Arthritis Rheumatol.* 67, 1062–1073. <https://doi.org/10.1002/art.38990>.
- Masuda, M., Miyazaki-Anzai, S., Levi, M., Ting, T.C., and Miyazaki, M. (2013). PERK-eIF2 α -ATF4-CHOP signaling contributes to TNF α -induced vascular calcification. *J. Am. Heart Assoc.* 2, e000238. <https://doi.org/10.1161/jaha.113.000238>.
- Miao, J., Ling, A.V., Manthena, P.V., Gearing, M.E., Graham, M.J., Crooke, R.M., Croce, K.J., Esquejo, R.M., Clish, C.B., Vicent, D., and Biddinger, S.B. (2015). Flavin-containing monooxygenase 3 as a potential player in diabetes-associated atherosclerosis. *Nat. Commun.* 6, 6498. <https://doi.org/10.1038/ncomms7498>.
- Nagatomo, Y., and Tang, W.H.W. (2015). Intersections between microbiome and heart failure: revisiting the gut hypothesis. *J. Card. Fail.* 21, 973–980. <https://doi.org/10.1016/j.cardfail.2015.09.017>.
- Onat, U.I., Yildirim, A.D., Tufanli, Ö., Çimen, I., Kocatürk, B., Veli, Z., Hamid, S.M., Shimada, K., Chen, S., Sin, J., et al. (2019). Intercepting the lipid-induced integrated stress response reduces atherosclerosis. *J. Am. Coll. Cardiol.* 73, 1149–1169. <https://doi.org/10.1016/j.jacc.2018.12.055>.
- Organ, C.L., Li, Z., Sharp, T.E., III, Polhemus, D.J., Gupta, N., Goodchild, T.T., Tang, W.H.W., Hazen, S.L., and Lefer, D.J. (2020). Nonlethal inhibition of gut microbial trimethylamine N-oxide production improves cardiac function and remodeling in a murine model of heart failure. *J. Am. Heart Assoc.* 9, e016223. <https://doi.org/10.1161/jaha.119.016223>.
- Organ, C.L., Otsuka, H., Bhushan, S., Wang, Z., Bradley, J., Trivedi, R., Polhemus, D.J., Tang, W.W., Wu, Y., Hazen, S.L., and Lefer, D.J. (2016). Choline diet and its gut microbe-derived metabolite, trimethylamine N-oxide, exacerbate pressure overload-induced heart failure. *Circ. Heart Fail.* 9, e002314. <https://doi.org/10.1161/circheartfailure.115.002314>.
- Pakshir, P., and Hinz, B. (2018). The big five in fibrosis: macrophages, myofibroblasts, matrix, mechanics, and miscommunication. *Matrix Biol.* 68–69, 81–93. <https://doi.org/10.1016/j.matbio.2018.01.019>.
- Pakshir, P., Noskovicova, N., Lodyga, M., Son, D.O., Schuster, R., Goodwin, A., Karvonen, H., and Hinz, B. (2020). The myofibroblast at a glance.

- J. Cell Sci. 133, jcs227900. <https://doi.org/10.1242/jcs.227900>.
- Patrone, V., Puglisi, E., Cardinali, M., Schnitzler, T.S., Svegliati, S., Festa, A., Gabrielli, A., and Morelli, L. (2017). Gut microbiota profile in systemic sclerosis patients with and without clinical evidence of gastrointestinal involvement. *Sci. Rep.* 7, 14874. <https://doi.org/10.1038/s41598-017-14889-6>.
- Piera-Velazquez, S., Mendoza, F.A., and Jimenez, S.A. (2016). Endothelial to mesenchymal transition (EndoMT) in the pathogenesis of human fibrotic diseases. *J. Clin. Med.* 5, 45. <https://doi.org/10.3390/jcm5040045>.
- Romano, K.A., Martinez-del Campo, A., Kasahara, K., Chittim, C.L., Vivas, E.I., Amador-Noguez, D., Balskus, E.P., and Rey, F.E. (2017). Metabolic, epigenetic, and transgenerational effects of gut bacterial choline consumption. *Cell Host Microbe* 22, 279–290.e7. <https://doi.org/10.1016/j.chom.2017.07.021>.
- Rudraiah, S., Moscovitz, J.E., Donepudi, A.C., Campion, S.N., Slitt, A.L., Aleksunes, L.M., and Manautou, J.E. (2014). Differential Fmo3 gene expression in various liver injury models involving hepatic oxidative stress in mice. *Toxicology* 325, 85–95. <https://doi.org/10.1016/j.tox.2014.08.013>.
- Schugar, R.C., Shih, D.M., Warriar, M., Helsley, R.N., Burrows, A., Ferguson, D., Brown, A.L., Gromovsky, A.D., Heine, M., Chatterjee, A., et al. (2017). The TMAO-producing enzyme flavin-containing monooxygenase 3 regulates obesity and the beiging of white adipose tissue. *Cell Rep.* 19, 2451–2461. <https://doi.org/10.1016/j.celrep.2017.05.077>.
- Shih, D.M., Wang, Z., Lee, R., Meng, Y., Che, N., Charugundla, S., Qi, H., Wu, J., Pan, C., Brown, J.M., et al. (2015). Flavin containing monooxygenase 3 exerts broad effects on glucose and lipid metabolism and atherosclerosis. *J. Lipid Res.* 56, 22–37. <https://doi.org/10.1194/jlr.m051680>.
- Shih, D.M., Zhu, W., Schugar, R.C., Meng, Y., Jia, X., Miikeda, A., Wang, Z., Zieger, M., Lee, R., Graham, M., et al. (2019). Genetic deficiency of Flavin-containing monooxygenase 3 (Fmo3) protects against thrombosis but has only a minor effect on plasma lipid levels—brief report. *Arterioscler. Thromb. Vasc. Biol.* 39, 1045–1054. <https://doi.org/10.1161/atvbaha.119.312592>.
- Shimizu, M., Origuchi, Y., Ikuma, M., Mitsuhashi, N., and Yamazaki, H. (2015). Analysis of six novel flavin-containing monooxygenase 3 (FMO3) gene variants found in a Japanese population suffering from trimethylaminuria. *Mol. Genet. Metab. Rep.* 5, 89–93. <https://doi.org/10.1016/j.ymgmr.2015.10.013>.
- Skaug, B., Khanna, D., Swindell, W.R., Hinchcliff, M.E., Frech, T.M., Steen, V.D., Hant, F.N., Gordon, J.K., Shah, A.A., Zhu, L., et al. (2020). Global skin gene expression analysis of early diffuse cutaneous systemic sclerosis shows a prominent innate and adaptive inflammatory profile. *Ann. Rheum. Dis.* 79, 379–386. <https://doi.org/10.1136/annrheumdis-2019-215894>.
- Sobolewski, P., Maślińska, M., Wiecezorek, M., Łagun, Z., Malewska, A., Roszkiewicz, M., Nitskovich, R., Szymańska, E., and Walecka, I. (2019). Systemic sclerosis—multidisciplinary disease: clinical features and treatment. *Reumatologia* 57, 221–233. <https://doi.org/10.5114/reum.2019.87619>.
- Tabib, T., Huang, M., Morse, N., Papazoglou, A., Behera, R., Jia, M., Bulik, M., Monier, D.E., Benos, P.V., Chen, W., et al. (2021). Myofibroblast transcriptome indicates SFRP2hi fibroblast progenitors in systemic sclerosis skin. *Nat. Commun.* 12, 4384. <https://doi.org/10.1038/s41467-021-24607-6>.
- Tang, W.W., Wang, Z., Kennedy, D.J., Wu, Y., Buffa, J.A., Agatista-Boyle, B., Li, X.S., Levison, B.S., and Hazen, S.L. (2015). Gut microbiota-dependent trimethylamine N-oxide (TMAO) pathway contributes to both development of renal insufficiency and mortality risk in chronic kidney disease. *Circ. Res.* 116, 448–455. <https://doi.org/10.1161/circresaha.116.305360>.
- Tang, W.W., Wang, Z., Levison, B.S., Koeth, R.A., Britt, E.B., Fu, X., Wu, Y., and Hazen, S.L. (2013). Intestinal microbial metabolism of phosphatidylcholine and cardiovascular risk. *N. Engl. J. Med.* 58, 549–558. <https://doi.org/10.1016/j.jvs.2013.06.007>.
- Tsoi, L.C., Iyer, M.K., Stuart, P.E., Swindell, W.R., Gudjonsson, J.E., Tejasvi, T., Sarkar, M.K., Li, B., Ding, J., Voorhees, J.J., et al. (2015). Analysis of long non-coding RNAs highlights tissue-specific expression patterns and epigenetic profiles in normal and psoriatic skin. *Genome Biol.* 16, 24. <https://doi.org/10.1186/s13059-014-0570-4>.
- Tsou, P.S., Palisoc, P.J., Ali, M., Khanna, D., and Sawalha, A.H. (2021). Genome-wide reduction in chromatin accessibility and unique transcription factor footprints in endothelial cells and fibroblasts in Scleroderma skin. *Arthritis Rheumatol.* 73, 1501–1513. <https://doi.org/10.1002/art.41694>.
- Varga, J., and Abraham, D. (2007). Systemic sclerosis: a prototypic multisystem fibrotic disorder. *J. Clin. Invest.* 117, 557–567. <https://doi.org/10.1172/jci31139>.
- Varga, J., and Marangoni, R.G. (2017). Dermal white adipose tissue implicated in SSc pathogenesis. *Nat. Rev. Rheumatol.* 13, 71–72. <https://doi.org/10.1038/nrrheum.2016.223>.
- Volkman, E.R., Hoffmann-Vold, A.-M., Chang, Y.-L., Jacobs, J.P., Tillisch, K., Mayer, E.A., Clements, P.J., Hov, J.R., Kummen, M., Midtvedt, Ø., et al. (2017). Systemic sclerosis is associated with specific alterations in gastrointestinal microbiota in two independent cohorts. *BMJ Open Gastroenter.* 4, e000134. <https://doi.org/10.1136/bmjgast-2017-000134>.
- Wang, Z., Klipfell, E., Bennett, B.J., Koeth, R., Levison, B.S., DuGar, B., Feldstein, A.E., Britt, E.B., Fu, X., Chung, Y.-M., et al. (2011). Gut flora metabolism of phosphatidylcholine promotes cardiovascular disease. *Nature* 472, 57–63. <https://doi.org/10.1038/nature09922>.
- Wang, Z., Roberts, A.B., Buffa, J.A., Levison, B.S., Zhu, W., Org, E., Gu, X., Huang, Y., Zamanian-Daryoush, M., Culley, M.K., et al. (2015). Non-lethal inhibition of gut microbial trimethylamine production for the treatment of atherosclerosis. *Cell* 163, 1585–1595. <https://doi.org/10.1016/j.cell.2015.11.055>.
- Watanabe, T., Frost, D.B., Mlakar, L., Heywood, J., da Silveira, W.A., Hardiman, G., and Feghali-Bostwick, C. (2019). A human skin model recapitulates systemic sclerosis dermal fibrosis and identifies COL22A1 as a TGFβ early response gene that mediates fibroblast to myofibroblast transition. *Genes* 10, 75. <https://doi.org/10.3390/genes10020075>.
- Witkowski, M., Weeks, T.L., and Hazen, S.L. (2020). Gut microbiota and cardiovascular disease. *Circ. Res.* 127, 553–570. <https://doi.org/10.1161/circresaha.120.316242>.
- Wu, W.-K., Chen, C.-C., Liu, P.-Y., Panyod, S., Liao, B.-Y., Chen, P.-C., Kao, H.-L., Kuo, H.-C., Kuo, C.-H., Chiu, T.H.T., et al. (2019). Identification of TMAO-producer phenotype and host–diet–gut dysbiosis by carnitine challenge test in human and germ-free mice. *Gut* 68, 1439–1449. <https://doi.org/10.1136/gutjnl-2018-317155>.
- Xu, M., Bhatt, D.K., Yeung, C.K., Claw, K.G., Chaudhry, A.S., Gaedigk, A., Pearce, R.E., Broeckel, U., Gaedigk, R., Nickerson, D.A., et al. (2017). Genetic and nongenetic factors associated with protein abundance of flavin-containing monooxygenase 3 in human liver. *J. Pharmacol. Exp. Therapeut.* 363, 265–274. <https://doi.org/10.1124/jpet.117.243113>.
- Zhang, L., Zhang, J., Yang, J., Ying, D., Lau, Y.I., and Yang, W. (2013). PriVar: a toolkit for prioritizing SNVs and indels from next-generation sequencing data. *Bioinformatics* 29, 124–125. <https://doi.org/10.1093/bioinformatics/bts627>.
- Zhang, W., Miikeda, A., Zuckerman, J., Jia, X., Charugundla, S., Zhou, Z., Kaczor-Urbanowicz, K.E., Magyar, C., Guo, F., Wang, Z., et al. (2021). Inhibition of microbiota-dependent TMAO production attenuates chronic kidney disease in mice. *Sci. Rep.* 11, 518. <https://doi.org/10.1038/s41598-020-80063-0>.
- Zhang, X., Chen, B.d., and Li, H. (2020). The gut microbiota: emerging evidence in autoimmune diseases. *Trends Mol. Med.* 26, 862–873. <https://doi.org/10.1016/j.molmed.2020.04.001>.
- Zhu, W., Gregory, J.C., Org, E., Buffa, J.A., Gupta, N., Wang, Z., Li, L., Fu, X., Wu, Y., Mehrabian, M., et al. (2016). Gut microbial metabolite TMAO enhances platelet hyperreactivity and thrombosis risk. *Cell* 165, 111–124. <https://doi.org/10.1016/j.cell.2016.02.011>.
- Zwick, R.K., Guerrero-Juarez, C.F., Horsley, V., and Plikus, M.V. (2018). Anatomical, physiological, and functional diversity of adipose tissue. *Cell Metabol.* 27, 68–83. <https://doi.org/10.1016/j.cmet.2017.12.002>.

STAR★METHODS

KEY RESOURCES TABLE

REAGENT or RESOURCE	SOURCE	IDENTIFIER
Antibodies		
p-PERK antibody	Cell Signaling	Cat# 3179; RRID: AB_2095853
PERK antibody	Cell Signaling	Cat# 3192; RRID: AB_2095847
Foxo1 antibody	Cell Signaling	Cat# 2880; RRID: AB_2106495
PECAM1 antibody	Abcam	Cat# ab124432; RRID: AB_2802125
GAPDH antibody	Santa Cruz	Cat# sc-47724; RRID: AB_627678
F-actin antibody	Abcam	Cat# ab205; RRID: AB_302794
Vinculin antibody	Cell Signaling	Cat# 4650; RRID: AB_10559207
Fibronectin-EDA antibody	Eosience	#5F0791
FMO3 antibody	Sigma-Aldrich	Cat# HPA013750; RRID: AB_1848968
α SMA antibody	Sigma	Cat# 5228; RRID: AB_262054
Collagen type I antibody	Southern Biotech	Cat# 1310-01; RRID: AB_2753206
Perilipin antibody	Abcam	Cat# ab61682; RRID: AB_944751
Adipocyte antibody	Abcam	Cat# ab26038; RRID: AB_448968
PPAR γ antibody	Cell Signaling	Cat# 2430; RRID: AB_823599
C/EBP α antibody	Santa Cruz	Cat# sc-61; RRID: AB_631233
Biological samples		
Skin biopsy specimens as listed in Table 2		
Adult healthy and SSc fibroblasts as listed in Table 2		
Chemicals, peptides, and recombinant proteins		
TMAO	Sigma-Aldrich	#317594
TMA	Sigma-Aldrich	#NMID778
Thapsigargin	Sigma-Aldrich	#T9033
TGF β 1	Pepro Tech	#100-21
PERK inhibitor	R&D Systems	#GSK 2606414
siRNA for PERK	Thermo Fisher Scientific	# 103,593
Experimental models: Cell lines		
Neonatal foreskin fibroblasts	Explanted in lab	
Human microvascular endothelial cells (HMVEC)	Lonza	#CC-2527

(Continued on next page)

Continued

REAGENT or RESOURCE	SOURCE	IDENTIFIER
Human adipose-derived stem cells (ADSCs)	Lonza	#PT-5006
Oligonucleotides		
Col1A1 primer Forward: 5'-TGGTGTGCAAGGTCCC-3' Reverse: 5'-CATTCCCTGAAGGCCAG-3'	Integrated DNA Technologies	N/A
Col1A2 primer Forward: 5'-GAGGGCAACAGCAGGTTCACTTA-3' Reverse: 5'-TCAGCACCACCGA TGTCCAA-3'	Integrated DNA Technologies	N/A
α SMA primer Forward: 5'-CAGGGCTGTTTTCCCATCCAT-3' Reverse: 5'-GCCATGTTCTATCGGGT ACTTC-3'	Integrated DNA Technologies	N/A
TG-B1 Forward: 5'-GCAGCACGTGGAGCTGTA-3' Reverse: 5'-CAGCCGGTTGCTGAGGTA-3'	Integrated DNA Technologies	N/A
Fn-EDA primer Forward:5'-TAAAGGACTGGCATTCACTGA-3' Reverse:5'-GTGCAAGGCAACCAC ACTGAC-3'	Integrated DNA Technologies	N/A
CD31 primer Target seq: 5'GAGCACCGTGCTGACCTCCAAATACCGTTAAGCTG GAGCCTCGGT GGCCATGCTTCTTGCCCTTGGCCCTCCCCCAGCCCTCCTCCCTTCTGACCCCGTACCCC CGTGGTCTTTGAATA3'	Bio-Rad Laboratories, Inc	N/A
CDH5 primer Target seq: 5'ATCTCCGCAATAGACAAGGACATAACACCACGAAA CGTGAAGTTC AAATTCATCTTGAATACTGAGAACAACCTTACCCTCACGGATAATCACGATAACACGGCCAACA TCACAGTCAAGTATGGGCAGTTGACCGGGAGC3'	Bio-Rad Laboratories, Inc	N/A
SNAI1 primer Target seq: 5'CTCCTGAGCTGAGGATCTCTGTTGTGGTATGACA GGCATGGAGTA ACTCTCATAGAGATACGGGAAATAACTGTATGTGTGTCAGTTGCTGTAGTTGGCTTTT TGGAGGCGTTGAAATGCTTCTTGACCAGGAAGGAGCGCGGCATCTTGC3'	Bio-Rad Laboratories, Inc	N/A
TAGLN primer Target seq:5' TGAGGACTATGGGGTCAAGACTGACATGTTCC AGACTGTGA CCTTTTGAAGGCAAAGACATGGCAGCAGTGAGAGGACCCTGATGGCTTTGGGCAGCTTGGC AGTGACCAAGAATGATGGGCACTACCGTGGAGATCCCAACTGTTTATGAAGAAAGCGCAGGA GCATAAGAGGGAATTCACAGAGAGCCAGCTGCAGGAGGGAAAGC3'	Bio-Rad Laboratories, Inc	N/A
ADIPOQ primer Target seq:5'TGATTTTCTCAAATTTCAACAAGTAGCTAAAGTC TGGCTATGCT CACAGTCTCACATCTGGTTGGGGTGGGCTCCTTACAGAACACGCTTTCACAGTTACCTAAACT CTCTGGGGCAGGGTTATCTTTTGGAAACCAGAGGCA3'	Bio-Rad Laboratories, Inc	N/A
PPAR γ primer Target seq:5'CACTGTCTGCAAACATATCACAAGAAATGACCATGG TTAGACACAG AGATGCCATTCTGGCCCAACTTTGGGATCAGCTCCGTGGATCTCTCCGTAATGGAAGACC ACTCCACTCCTTTGATATCAAGCCCTTCACTACTGTTGA3'	Bio-Rad Laboratories, Inc	N/A
FABP4 primer Target seq:5'GAAACAACAATATCTTTTGAACAATATATCCAC AGAATGTTGT AGAGTTCAATGCGAACTTCAGTCCAGGTCAACGTCCTTGGCTTATGCTCTCTATAAACTCTC GTGGAAGTGACGCTTTCATGA3'	Bio-Rad Laboratories, Inc	N/A
FMO1 primer Target seq:5'GTGTAATAAGTTACCACCACCAAGTGTCATGATAG AGGAAATTA TGAAGGAAAGAAAACAAGCCAGTTGGTTTGGCTTGTGCTACTGCAAGGCTTTACAATCAGAT TATATCACATACATAGATGAACTCCTGACCTATATCAATGCAAAA3'	Bio-Rad Laboratories, Inc	N/A
FMO3 primer Target seq:5'AAAAGTTACCATGGGGAAGAAAGTGGCCATCATT GGAGCTGGTG TGAGTGGCTTGGCCTCCATCAGGAGCTGTCTGGAAGAGGGGCTGGAGCCACCTGCTTTGAGA AGAGCAATGACATTGGGGCCTGT3'	Bio-Rad Laboratories, Inc	N/A
GAPDH primer Forward 5'-CATGAGAAGTATGACAACAGCCT-3' Reverse 5'-AGTCTTCCACGA TACCAAAGT-3'	Integrated DNA Technologies	N/A
Software and algorithms		
Prism	GraphPad Software	

RESOURCE AVAILABILITY

Lead contact

Further information and requests for resources and reagents should be directed to and will be fulfilled by the lead contact, John Varga (vargaj@med.umich.edu).

Materials availability

This study did not generate new unique reagents.

Data and code availability

- Analysis of multiple transcriptome datasets showing elevated expression of FMO3 in SSc skin biopsies consistent across five independent patient cohorts originate from NCBI GEO (GEO: GSE95065, GEO: GSE130955, GEO: GSE47162; summarized in [Table 1](#)).
- The paper does not report original codes or reagents. All codes or reagents used in this study are listed in the [Key resources table](#).
- Any additional information required to reanalyze the data reported in this paper is available from the [lead contact](#).

EXPERIMENTAL MODEL AND SUBJECT DETAILS

Cell culture and reagents

Fibroblasts were isolated from neonatal foreskin samples and maintained in Dulbecco's Modified Eagle Medium (DMEM) with 10% Fetal Bovine Serum (FBS) ([Fang et al., 2012](#)). Human microvascular endothelial cells (HMVEC) (from Lonza, Basel, Switzerland) were maintained in endothelial growth media (EGM-2). Human adipose-derived stem cells (ADSCs) from Lonza were maintained in ADSC growth medium ([Marangoni et al., 2015](#)). Fibroblasts were also derived from punch skin biopsies from patients with SSc and healthy adults volunteers by explantation, and used at low passage. For knockdown experiments, confluent fibroblasts or HMVECs were transfected with PERK siRNA or scrambled control siRNA for 72 h, and downregulation of cellular PERK was confirmed by immunoblotting. Trimethylamine (TMA), trimethylamine-*N*-oxide (TMAO) and thapsigargin were purchased from Sigma-Aldrich (St. Louis, MO, USA). Human TGF- β 1 was purchased from PeproTech (Cranbury, NJ, USA) and the PERK inhibitor AMG PERK44 from R&D Systems (Minneapolis, MN, USA). siRNA for PERK was from Thermo Fisher Scientific (Waltham, MA, USA).

Quantitative real-time PCR (qPCR)

RNA was isolated from confluent foreskin fibroblasts, HMVEC and ADSCs using Quick-RNA MiniPrep Kit (Zymo Research, Irvine, CA), reverse transcribed to cDNA and subjected to qPCR ([Marangoni et al., 2015](#)). The primers ([Table S1](#)) for collagen 1a1 (Col1a1, encoded to *COL1A1*), collagen 1A2 (Col1A2, encoded by *COL1A2*), α -smooth muscle actin (α SMA, encoded by *ACTA2*), transforming growth factor β 1 (TGF- β 1, encoded by *TGFB1*), fibronectin containing extra domain A (*Fn-EDA*), CD31 (*PECAM1*), VE-cadherin (*CDH5*), adiponectin (*ADIPOQ*), peroxisome proliferator-activated receptor γ (*PPARG*), fatty acid-binding protein 4 (*FABP4*), *FM O 1*, *FM O 3* and *GAPDH* were purchased from Bio-Rad (Hercules, CA). Gene expression levels were normalized with GAPDH and calculated using the $2^{-\Delta\Delta C_t}$ formula ([Marangoni et al., 2015](#)).

Measurement of collagen, fibronectin and TGF- β 1 secretion

Fibroblasts were grown in 24-well plates, and at confluence incubated in media with TMAO (50–200 μ M) or TGF- β 1 (10 ng/mL) for up to 72 h. Levels of procollagen I, fibronectin, and TGF- β 1 in the culture media were determined by ELISA (R&D Systems, Minneapolis, MN). Each experiment was performed in triplicate.

Immunofluorescence confocal microscopy

Healthy control and SSc skin fibroblasts at low passage were seeded on 8-well Lab-Tek II chamber glass slides (Nalgen Nunc, Naperville, IL, USA) and incubated in serum-free culture media with 0.1% BSA for 24 h, followed by fresh media with indicated concentrations of TMAO for 48 h. Cells were fixed, permeabilized, and incubated with primary antibodies followed by Alexa-fluor-labelled secondary antibodies (Invitrogen, Carlsbad, CA, USA). Nuclei were identified using 4,6-diamidino-2-phenylindole (DAPI). Immunofluorescence was evaluated under a Nikon C2 or A1Si confocal microscope.

Immunoblot analysis

Whole cell lysates were subjected to immunoblot analysis using antibodies for phospho-PERK (Thr980; Cell Signaling, Danvers, MA), FMO3, PERK (Cell Signaling), Foxo1 (Cell Signaling), transgelin (TGLN) (Abcam), PECAM-1 or GAPDH (both from Santa Cruz, Dallas, TX). Electrophoretic bands were detected using

enhanced chemiluminescence reagents (Pierce Biotechnology, Rockford, IL), and band intensities were quantified with ImageJ software.

RNA sequencing

Total RNA was isolated from HMVECs treated with or without TMAO for 48 h using RNeasy Mini kits (QIAGEN). RNA sequencing was performed by the University of Michigan Advanced Genomics Core and subjected to 150 paired end cycles on the NovaSeq-6000 platform (Illumina). Data were pre-filtered to remove genes with 0 counts in all samples. Differential gene expression analysis was performed using DESeq2, using a negative binomial generalized linear model (thresholds: linear fold change >1.5 or < -1.5, Benjamini-Hochberg FDR (Padj) < 0.05). Functional analysis, including candidate pathways activated or inhibited in comparison(s) and GO-term enrichments, was performed using iPathway Guide (Advaita) (iPathwayGuide).

Cell migration assays

To measure the effect of TMAO on cell migration, HMVECs were plated in 96-well Image Lock Microplates. When the cultures reached at confluence, scratch wounds were created (Tsou et al., 2021). Media were replaced with EGM-2 with 0.1% FBS, with or without TMAO (50 μ M), and at indicated times, plates were placed in IncuCyte (Sartorius, Ann Arbor, MI) to acquire data and images, which were quantified using the Analysis module in the IncuCyte software (Tsou et al., 2021).

ADSC differentiation assays

Human ADSCs were maintained in growth medium (ADSC-GM; Lonza). At low passage (passage 2–4), cells were seeded in 12-well plates (1×10^5 cells/well) and incubated in PBM-2 growth medium (Lonza), followed by adipocyte differentiation medium (PBM-2/PDM; Lonza). At day 10 of differentiation, when the cells have acquired the characteristic adipocyte morphology with rounded shape and accumulation of prominent intracytoplasmic lipid droplets, TMAO or TGF- β 1 was added to the media. After 72 h, cultures were incubated with Oil Red O (Abcam) and visualized by phase-contrast microscopy (Marangoni et al., 2015).

Single-cell RNA-sequencing (scRNA-seq) analysis in skin biopsies

To generate single cell suspensions for single-cell RNA sequencing (scRNA-seq), skin biopsies from patients with SSC ($n = 6$) and healthy controls ($n = 2$) were minced, digested in 0.2% collagenase II (Life Technologies) and 0.2% collagenase V (Sigma) for 60 min, and strained through a 70 μ M mesh. Samples were analyzed by the University of Michigan Advanced Genomics Core on the 10X Chromium system. Libraries were sequenced on the Illumina NovaSeq 6000 sequencer to generate 151-bp paired end reads. Adapter trimming and quality control procedures were performed (Li et al., 2014; Tsoi et al., 2015). The reads were mapped using STAR (Zhang et al., 2013) to human build GRCh37, and gene expression levels were quantified and normalized by HTSeq (Anders et al., 2015) and DESeq2 (Love et al., 2014), respectively. Negative binomial model in DESeq2 were used to conduct differential expression analysis. Data processing including quality control, read alignment and gene quantification used the 10X Cell Ranger software. Seurat was used for normalization, data integration, and clustering analysis (Butler et al., 2018).

The R package Seurat (v3.1.2) was used to cluster the cells in the merged matrix. Cells with less than 500 transcripts or 100 genes or more than $1e5$ transcripts or 15% of mitochondrial expression were first filtered out as low-quality cells. The NormalizeData function was used to normalize the expression level for each cell with default parameters. The FindVariableFeatures function was used to select variable genes with default parameters. The ScaleData function was used to scale and center the counts in the dataset. Principal component analysis (PCA) was performed on variably expressed genes. The RunHarmony function from the Harmony package was applied to remove potential batch effect among samples processed in different batches. Uniform Manifold Approximation and Projection (UMAP) dimensional reduction was performed using the RunUMAP function. The clusters were obtained using the FindNeighbors and FindClusters functions with the resolution set to 0.6. The cluster marker genes were found using the FindAllMarkers function. The cell types were annotated by overlapping the cluster markers with published fibroblast markers.

Skin histology and immunochemistry

Demographic and clinical features of subject donating skin biopsy specimens are listed in [Table 1](#). Four-micron-thick sections of formalin-fixed, paraffin-embedded biopsy samples were used for immunolabeling ([Marangoni et al., 2015](#)). Following antigen retrieval (DAKO Envision Flex Target Retrieval Solution, low pH), slides were incubated with anti-FMO3 antibodies (rabbit polyclonal, Millipore/Sigma-Aldrich, catalog # HPA013750) at 1:100 dilution for 30 min, followed by HRP-conjugated secondary antibodies, and visualized with diaminobenzidine substrate, and counterstained with hematoxylin. Immunopositive cells in the dermis were counted in 3 randomly selected high-power fields (40X) in a blinded manner. One-way ANOVA was used for statistical significance analysis. Negative controls stained without primary antibody were used to confirm specificity.

Quantification of histone H3 modifications

To evaluate histone modifications elicited by TMAO treatment of fibroblasts, Histone H3 Modification assays were performed using EpiQuik™ kits from Epigentek (Farmingdale, NY, USA). The multiplex assay kits measure histone modifications and require cellular histone isolation using EpiQuik™ total histone extraction kits (Epigentek).

QUANTIFICATION AND STATISTICAL ANALYSIS

Data are presented for each group as mean \pm S.E.M. For comparison between 2 groups, a two-tailed Student's t-test was used. For comparison for three or more groups, a one-way ANOVA and Tukey's multiple comparison test was performed. Statistical analysis was performed using GraphPad Prism (La Jolla, CA). Probability values <0.05 were considered statistically significant.